ACS OMEGA

Open Access

http://pubs.acs.org/journal/acsodf

Article

Geochemical and Organic Petrological Characteristics of the Bituminous Carbonate Succession (Upper Cretaceous Shu'ayb Formation) in Northern Jordan: Implications for Organic Matter Input and Paleosalinity, Paleoredox, and Paleoclimatic Conditions

Mohammed Hail Hakimi,* Mohammad Alqudah, Malik M. Momani, Danish Zahir, Ahmed Abd El Aal, Mohamed M. El Nady, Afikah Rahim, and Baleid Ali Hatem

Cite This: *ACS Omega* 2024, 9, 27458−27479

Read Online

ACCESS | Metrics & More | Article Recommendations

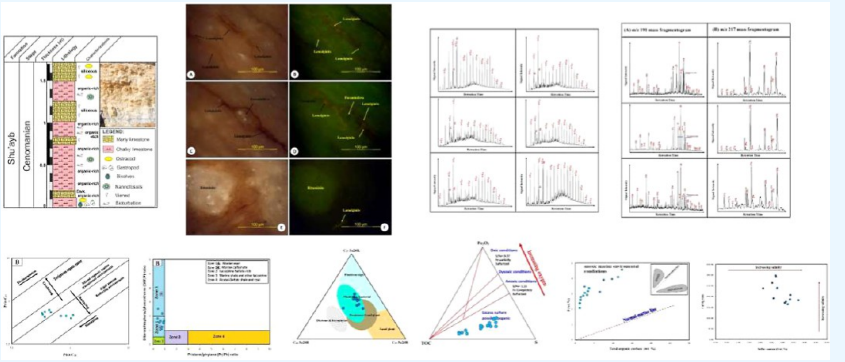

ABSTRACT: Bituminous carbonate rocks of the Upper Cretaceous Shu'ayb Formation from the Ajloun outcrop in Northern Jordan were geochemically and petrologically analyzed in this study. This study integrates kerogen microscopy results with geochemical results (i.e., biomarker, stable carbon isotope, and major elemental compositions) to understand the organic matter (OM) inputs and to reveal the dispositional setting and its effect on the occurrence of OM. The Shu'ayb bituminous carbonate rocks have high total organic carbon (TOC) and sulfur (S) contents, with average values of 12.3 and 4.59 wt %, respectively, indicating redox conditions during their precipitation. The high abundance of alginite (i.e., *lamalginite*) in the Shu'ayb bituminous carbonate sediments is a further evidence for redox conditions. The finding of mainly marine-derived OM was also demonstrated by the biomarker distribution and carbon isotope composition. The biomarkers are represented by a narrow Pr/Ph ratio of up to 0.97, abundance of tricyclic terpanes, and high C_{27} regular sterane, indicating that the OM was primarily derived from phytoplankton algae, along with small amounts of land plant-derived materials, and were accumulated under reducing conditions. The studied Shu'ayb bituminous carbonate facies is composed of mainly calcium (CaO; average, 45.10 wt %), with significant amounts of silicon (Si_2O_3; avg., 9.35 wt %), aluminum (Al_2O_3; avg., 6.91 wt %), and phosphorus (P_2O_3; avg., 1.47 wt %) and low amounts of iron (Fe_2O_3) and titanium (TiO_2) of less than 1 wt %, indicating that the detrital influx was low in an open water depth system with higher primary bioproductivity. The geochemical proxy suggests that the Shu'ayb bituminous carbonate facies was established in a saline water environment, with Ca/Ca + Fe and S/TOC values of more than 0.9 and 0.50, respectively, which could be attributed to the increase in reducing conditions of the water column. The chemical index of alteration values of more than 0.8 also indicate that the Shu'ayb bituminous carbonate facies formed during warm and humid climatic conditions, thereby resulting in intense subaerial weathering.

1. INTRODUCTION

Organic matter (OM)-rich fine-grained rocks such as shale, mudrock, and carbonate have been increasingly considered as conventional and unconventional oil and gas resources.[1−3] These organic-rich sedimentary rocks were deposited in both marine and continental environments and have recently become an essential target resource for oil exploration in petroleum-

Received: March 16, 2024
Revised: May 17, 2024
Accepted: May 17, 2024
Published: June 12, 2024

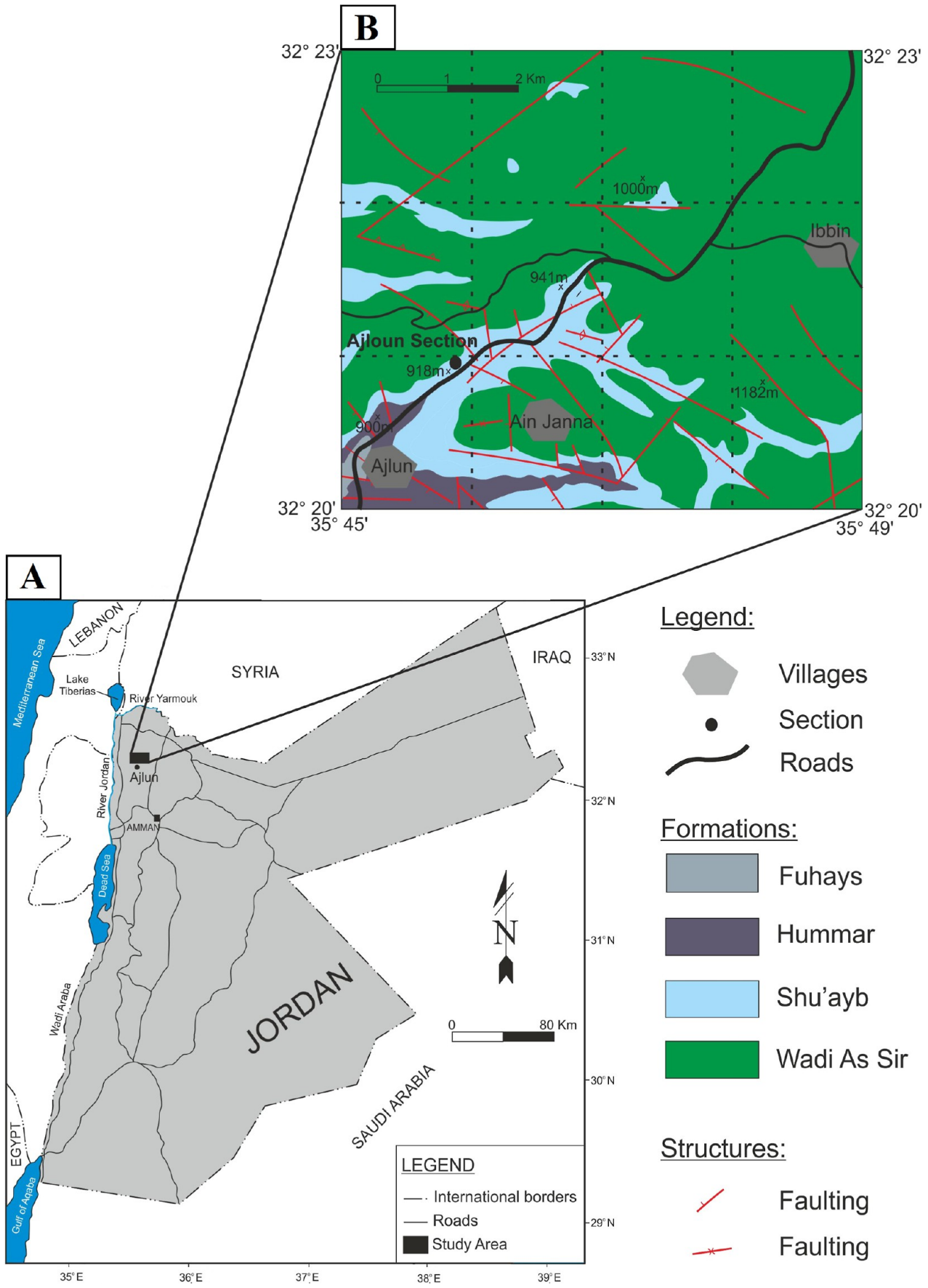

Figure 1. (A) Geographic map of Jordan showing the Wadi Ajloun area in Northern Jordan and (B) the Ajloun area showing the geological exposures of various geological formations.

https://doi.org/10.1021/acsomega.4c02582
ACS Omega 2024, 9, 27458−27479

producing sedimentary basins of the world.[2,4] Most of the fine-grained organic-rich sediments contain noticeable quantities of more than three percent OM and were deposited under redox conditions.[5−7] However, several environmental factors such as water column oxygenation levels and climatic conditions together with other factors of weathering, clay content, sedimentation rates, and sea-level change have seriously impacted the OM in these organic-rich sediments.[8−11]

This study focuses on Jordanian oil shales, which possess resources of more than 65 billion tons of oil shale deposits.[12] Jordanian basins include a number of OM-rich horizons, such as the Upper Cretaceous bituminous sediments.[13−19] The Upper Cretaceous (OAE2) sediments are characterized by fine-grained organic-rich facies of black shale, calcareous shale, and marl and are considered key factors for water column bioproductivity and preservation of OM during reducing conditions.[13−17]

The Shu'ayb Formation in Northern Jordan was deposited during this time. The Upper Cretaceous Shu'ayb bituminous carbonates in northern basins of Jordan have recently attracted researchers' attention and upstream exploration ventures due to the superior source rocks found in these basins and oil generation potential, with the high total organic carbon (TOC) content reaching 12 wt %.[19] The Shu'ayb organic-rich carbonate sediments are enriched in sapropelic OM and belong to one of the high-quality oil-source rocks in Northern Jordan's basins.[19] A preliminary study proposed that the bituminous carbonates mainly contain Types I and II kerogen, which can generate profitable amounts of sulfur-rich oil during the early mature stage of the oil window.[19]

Although previous works have focused on the geochemical assessment of the bituminous carbonate facies in the Shu'ayb Formation and its ability for oil generation potential,[19] little is known about the depositional environment factors and their implication for understanding the organic carbon accumulation in the Upper Cretaceous sequence in Northern Jordan. Therefore, the main objective of this study was to understand the source of OM, depositional environment factors (i.e., paleoredox, paleosalinity, and warm climatic conditions) that influenced the organic carbon productivity and preservation in the Shu'ayb bituminous carbonate rocks. In this case, the current study integrated geochemical results with new findings of biomarker and carbon isotope composition as well as inorganic geochemical studies of the bituminous carbonate rocks within the Upper Cretaceous Shu'ayb bituminous carbonate strata at the Ajloun outcrop, Northern Jordan, using multigeochemical techniques together with organic petrology.

2. GEOLOGICAL SETTING

Tectonic movements during Cenomanian time significantly influenced the depositional environment in the eastern part of Neo-Tythes. This shift can be documented in the sediments deposited during that time.[20]

In Jordan, a recognizable layer of organic-rich sedimentary rocks was deposited within the inner/midshelf overlaid by shallow subtidal to supratidal inner-shelf platform deposits.[21−23]

The study area is situated in the northwest of Amman, and the investigated site lies along the Ajloun-Irbid Road (Figure 1A). The area is characterized by a complex topography with steep reliefs. The elevation within the area ranges between 945 m in the northern part and 918 m above the sea level (ASL) in the southern part of the study area. However, numerous structural features such as folding and faulting in the study area indicate that the Ajloun area was subjected to different tectonic and structural movements; these movements led to the formation of the so-called Ajloun Dome.[21,24]

The Upper Cretaceous rocks are exposed in the Wadi Ajloun area, Northern Jordan, and consist of limestones, marly limestone, and soft marl which belong to the Ajloun Group.[25] The Ajloun Group is divided into formations, from bottom to top as follows: 1) Fuhays, 2) Hummar, 3) Shu'ayb, and 4) Wadi As Sir (refer to Figure 1B). A sequence of marls at the bottom (The Fuhays Formation), massive dolomitic limestone (Hummar Formation) in the middle and, chalky limestones and organic-rich chalky marls (Shu'ayb Formation) at the top were deposited during the early Cenomanian to the early Turonian age.[26]

The Ajloun section, which belongs to the Shu'ayb Formation (Figure 2), consists mainly of massive crystalline fossiliferous

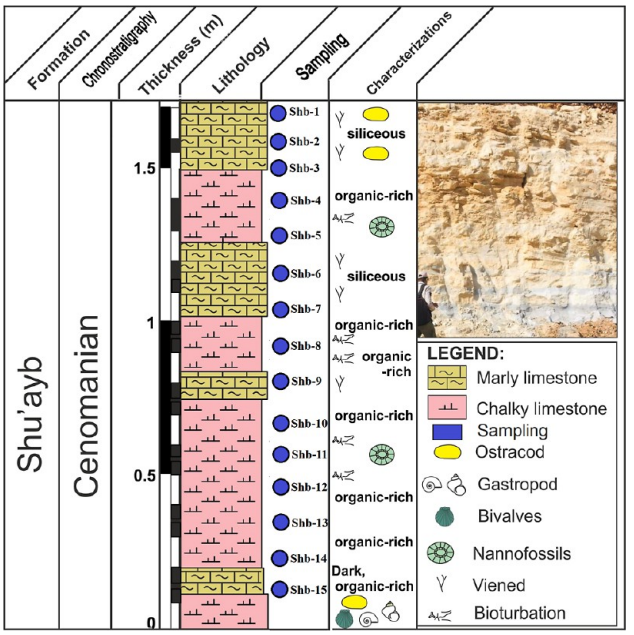

Figure 2. Sedimentary log and field photograph of the studied Shu'ayb Formation in the study area. The field photograph was taken by Mohammad Alqudah.

limestones at the bottom. White, hard chalk containing many fossil forms such as gastropods, ostracods, and bivalves is observed just below the organic-rich sediments. Layers of marly limestones characterized by a high concentration of OM and an abundance of macrofossils occur within the massive limestone layer (Figure 2). This layer underlies sequences of marls and limestones, which also include high organic carbon contents. Veins filled with siliceous-free crystals can be observed in siliceous chalk. Hard siliceous chalky limestones with moderate contents of microfossils such as ostracods become dominating upward.[24,27,28] This formation varies in thickness, starting from 3 m within the top part and the thickness increasing downward. The organic-rich beds contain varying amounts of bioturbations, alongside large fossils such as gastropods, burrows, and bivalves; these kinds of fossils were deposited mainly within a moderate to subtidal marine environment.[24] The Shu'ayb Formation in the study area has a total thickness from the base to the top around 3 m and comprises three beds enriched in OM, with a TOC content of up to 12.3 wt %.[19]

https://doi.org/10.1021/acsomega.4c02582
ACS Omega 2024, 9, 27458−27479

3. MATERIALS AND EXPERIMENTAL METHODS

A section from the Ajloun exposure in Wadi Ajloun, Northern Jordan, containing 15 bituminous carbonate samples of the Shu'ayb Formation was investigated (Figure 2). However, the pretreatment process was done on the samples by cleaning up the weathered surfaces prior to performing the geochemical and petrological analyses.

The ground bituminous carbonate samples were analyzed geochemically and by microscopic examination. Other investigations, including the TOC content, sulfur (S) content, carbon isotope composition, gas chromatography−mass spectrometry (GC−MS), and X-ray fluorescence (XRF) analysis, were conducted on the samples. These analyses were performed at different geochemical and organic petrological laboratories in the universities (i.e., University of Malaya in Malaysia, Al-Bayt University in Jordan, and Calgary University in Canada).

3.1. Microscopic Examinations. The whole bituminous carbonate samples underwent organic petrological examination and organic facies analysis using a standard polished block procedure,[29] as described in the following subsection. In this case, the entire rock volume of the samples was ground into small portions in the range 1.5−2 mm and then gathered with a SeriFix resin and a hardener agent. Then, the surface was smoothed by silicon carbide paper and alumina powder following the standard procedure of ASTM D2797-04. The resultant blocks were then examined using a LEICA DM4 microscope under white light with an oil-immersion medium, cross-polarized, and under UV light. The OM input and its morphology were examined under a fluorescence microscope using a mercury (Hg) lamp for the UV light analysis.

3.2. Organic Geochemical Analyses. The TOC and S contents and gas chromatography−mass spectrometry (GC−MS) were conducted on the samples. The analysis of TOC and S (weight percent) contents of finely milled (60 μm) 15 samples was performed by a LECO CS244 analyzer. Carbonate minerals were removed from the sample using 10% dilute hydrochloric acid.

Of these 15 samples, the free bitumen in the studied organic-rich samples was extracted from 10 crushed samples (30 g) using Soxhlet extraction for 72 h, with a mixed solvent of dichloromethane and methanol. The extracted bitumen was then fractioned into saturate, aromatic, and polar fractions using different polarity solvents and applying a medium-pressure liquid chromatography separation method.

Later, the saturated hydrocarbon fraction was analyzed using GC−MS to pick the biomarker compounds using an Agilent GC−MS HP 5975B MSD equipped with a flame ionization detector. The capillary column of the GC−MS apparatus had a diameter of 0.32 mm, a length of 30 m, and a film thickness of 0.25 μm. In the GC−MS furnace, the samples were heated from 40 to 300 °C (the rate was approximately 4 °C/min), and then the temperature was fixed at 300 °C for 30 min. Finally, the saturated HC fraction was separated into biomarker compounds, including normal alkanes, hopanoids, isoprenoids, steranes, and terpanes, which were detected and quantified from their peak heights from m/z 85, 191, and 217 (see Appendix).

In addition, 15 bituminous carbonate samples from the Shu'ayb Formation in the Ajloun section were also subjected to stable carbon isotope analysis. The samples were crushed and powdered prior to analysis on a mass spectrometer at Calgary University (Canada). All values reported here are based on the standard δ-notation relative to the Vienna PDB (Pee Dee Belmenite) standard.

3.3. XRF Analysis. The presence of inorganic compounds such as trace metals (e.g., silicon, manganese, aluminum, and iron) and the elemental compositions of the Shu'ayb bituminous carbonate samples were determined by XRF analysis at the Water, Environment and Arid Regions Research Center, Al Al-Bayt University. In this analysis, the bulk 15 bituminous carbonate ground samples were passed through 200 meshes and analyzed using an XRF apparatus to measure the main major oxides (i.e., CaO, SiO_2, Al_2O_3, Fe_2O_3, K_2O, MgO, P_2O_5, Na_2O, and TiO_2).

4. RESULTS

4.1. Microscopic Features. Microscopic examinations were performed on Shu'ayb bituminous carbonate samples under white and UV light, as shown in Figures 3 and 4,

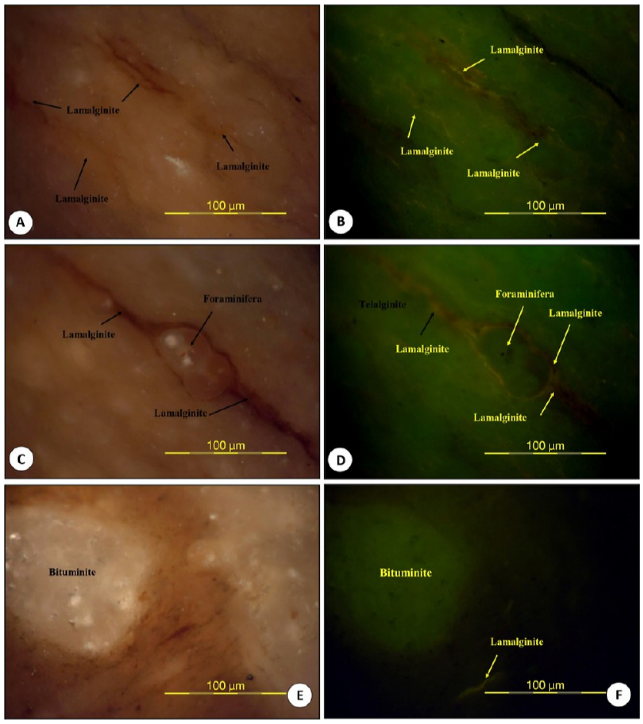

Figure 3. Photomicrographs of the investigated organic-rich carbonates of the Upper Cretaceous Shu'ayb Formation, under reflected light and fluorescence under UV, with a field width of 0.2 mm, showing (A−D) alginite, mainly lamalginite, and (E and F) unstructured bituminite OM associated with lamalginite algae.

respectively. A high percentage of liptinite and a smaller quantity of vitrinite macerals are the dominant organofacies (Figure 3). Liptinites include structured and unstructured OM, with fluorescence colors fluctuating from greenish to orange and yellow (Figure 3B,D,F). However, alginite is the most common group found within the liptinites (Figure 3A−F), which appeared as a lamalginite algae based on its morphology. Lamalginite arose from algae and was placed in lamellae (Figure 3A−F). However, the lamalginite assemblages are assumed to have formed in aquatic medium.[17,29−31] Other unstructured OM such as bituminite was also recognized in the studied Shu'ayb carbonate samples (Figure 3E), which have a greenish fluorescence under UV light (Figure 3F).

https://doi.org/10.1021/acsomega.4c02582
ACS Omega 2024, 9, 27458−27479

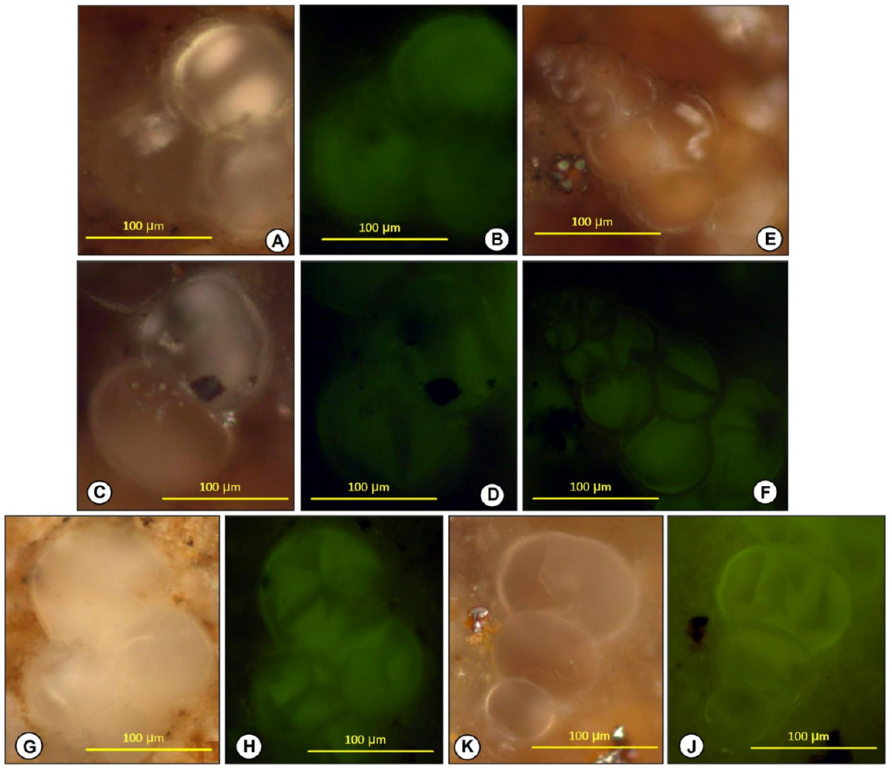

Figure 4. Photomicrographs of the investigated organic-rich carbonates of the Upper Cretaceous Shu'ayb Formation, under reflected white and blue lights, with a field width of 0.2 mm, showing different types of planktonic foraminifera assemblages (A,B) *Globigerina connecta* sp., (C,D) *Orbulina bilobata* sp., (E,F) *Heterohelix* sp., (G,H) *Globigerina falconensis* sp., and (K,J) *Orbulina bilobata* sp.

In addition, foraminifera assemblages are dominant in the studied Shu'ayb samples, which were infused with the mineral matrix and characterized by a greenish fluorescence when examined under UV light (Figure 4). The common identified foraminifera are planktonic foraminifera (p) species, including *Globigerina connecta* sp., *Globigerina falconensis* sp., *Orbulina bilobata* sp., and *Heterohelix* sp. (Figure 4).

4.2. TOC and Sulfur Contents. TOC content is exclusively used to understand organic-richness during deposition, conventionally reported as a function of preservation of OM during reducing environmental conditions.

In this study, the TOC results show that all samples are rich and exhibit high values, ranging from 1.20 to 12.30 wt % (Table 1); most of the samples have a TOC range of 2.45−12.30 wt %, whereas four samples exhibited relatively low TOC values between 1.20 and 1.50 wt % (Table 1). Consequently, all the examined bituminous carbonate samples of the Shu'ayb Formation were accumulated under redox conditions. However, the measured high TOC content alone is insufficient to assess the redox conditions; accordingly, biomarker fingerprints also pointed to the source of OM and its environmental condition, which are explained in the following sections.

The total sulfur (TS) content in the Shu'ayb bituminous carbonate samples was also measured and ranged from 2.09 to 4.59 wt % (Table 1). Most of the analyzed samples have TS values of more than 2.5 wt %, while other limited samples show lower TS values between 2.09 and 2.40 wt % (Table 1). However, the S content usually distinguishes marine environments from nonmarine.[32,33] In this case, Wei and Algeo[33] indicated that the sediments deposited within marine environments show the sulfur content ranges from 0.48 to 1.69 wt %, and TOC contents are more than 2%, while the sediments deposited in freshwater environments have the values of TS range from 0.03 to 0.16 wt %. Accordingly, the Shu'ayb bituminous carbonate facies was mainly deposited in a marine setting, with a high S content of up to 4.59 wt % (Table 1).

4.3. Stable Carbon Isotope ($\delta^{13}C$) Composition. The carbon isotope ($\delta^{13}C$) composition of OM in the Shu'ayb bituminous carbonate facies was determined, and the analyzed samples revealed a range of $\delta^{13}C$ values for OM from −28.90 to −31.40‰, as detailed in Table 1. The $\delta^{13}C$ values can be distinguished into nonmarine and marine OM inputs, as suggested by Sofer[34] and Summons et al.[35] Specifically, lower $\delta^{13}C$ values (less negative) revealed the terrigenous origin, while higher lighter $\delta^{13}C$ values (more negative) suggested marine OM source. Consequently, the examined bituminous carbonate samples of the Shu'ayb Formation appeared to be of marine origin, with little input from terrigenous OM.

4.4. Major Oxides. The abundances of major oxides, with their geochemical ratios, are given in Table 1. The studied Shu'ayb bituminous carbonate samples have higher CaO, SiO_2, and Al_2O_3 when compared with other oxides (Table 1). The amount of CaO, SiO_2, and Al_2O_3 in most of the studied samples range from 12.03 to 63.29 wt %, from 11.26 to 44.57 wt %, and from 11.26 to 44.57 wt %, respectively (Table 1). The Shu'ayb carbonate samples are also depleted in Fe_2O_3, P_2O_5, NaO_2, MgO, K_2O, TiO_2, and MnO, respectively (Table 1). However, Al_2O_3 and SiO_2 are strongly correlated, as observed from relatively low Si/Al ratios of 1.02 and 1.66 (Table 1) and the positive correlation between Al_2O_3 and SiO_2 (Figure 5A), suggesting that Si in the studied samples was mainly from clay minerals rather than from the quartz mineral.[36−38] It appears that the presence of clay minerals in the analyzed samples is confirmed by the positive correlations between both Al_2O_3 and

https://doi.org/10.1021/acsomega.4c02582
ACS Omega 2024, 9, 27458−27479

Table 1. Geochemical Results of the Analyzed Bituminous Carbonate Rock throughout the Upper Cretaceous Shu'ayb Formation from the Ajloun Outcrop, Including TOC and TS Contents, Stable Carbon Isotope ($\delta^{13}C$) Composition, and Most Major Oxides (%)[a]

					major oxides (%)																	
samples ID	TOC wt %	TS wt %	TS/TOC	$\delta^{13}C_{org}$ (‰)	CaO	SiO_2	Al_2O_3	P_2O_5	Fe_2O_3	Na_2O	MgO	K_2O	TiO_2	MnO	Si/Al	P/Ti	K/Al	Ti/Al	Al/Ti	100 × Mg/Al	Ca/(Ca + Fe)	Al/(Al + Fe)	CAI
Shb-1	1.21	2.40	1.98	−31.1	42.2	10.72	7.59	1.95	1.01	0.34	0.24	0.31	0.26	0.02	1.41	7.50	0.04	0.03	29.19	3.16	0.98	0.88	0.92
Shb-2	1.44	2.62	1.82	−28.9	52.18	7.12	5.37		0.64	0.52	1.35	0.31	0.15	0.02	1.33		0.06	0.03	35.80	25.14	0.99	0.89	0.87
Shb-3	7.52	3.92	0.52	−29.1	51.59	7.11	5.34		0.63	0.51	1.34	0.31	0.13	0.02	1.33		0.06	0.02	41.08	25.09	0.99	0.89	0.87
Shb-4	3.15	2.94	0.93	−31.1	40.94	10.91	7.66	1.95	1.00	0.32	0.24	0.31	0.28	0.02	1.42	6.96	0.04	0.04	27.36	3.13	0.98	0.88	0.92
Shb-5	1.20	2.09	1.74	−31.1	43.04	8.5	6.88	1.53	0.87	0.31	0.23	0.29	0.23	0.02	1.24	6.65	0.04	0.03	29.91	3.34	0.98	0.89	0.92
Shb-6	2.45	3.48	1.42	−30.9	47.44	8.56	7.09	1.02	0.89	0.3	0.18	0.26	0.23	0.02	1.21	4.43	0.04	0.03	30.83	2.54	0.98	0.89	0.93
Shb-7	11.30	4.11	0.36	−31.4	47.95	8.89	7.21	1.04	0.88	0.34	0.2	0.27	0.23	0.02	1.23	4.52	0.04	0.03	31.35	2.77	0.98	0.89	0.92
Shb-8	2.13	2.89	1.36	−30.3	36.44	10.27	7.32	1.75	0.99	0.27	0.19	0.28	0.23	0.02	1.40	7.61	0.04	0.03	31.83	2.60	0.97	0.88	0.93
Shb-9	3.34	3.19	0.96	−30.3	35.76	9.3	7.05	1.63	1.00	0.25	0.15	0.27	0.23	0.02	1.32	7.09	0.04	0.03	30.65	2.13	0.97	0.88	0.93
Shb-10	9.70	3.98	0.41	−30.1	47.6	9.28	6.99	1.62	0.95	0.4	0.26	0.25	0.21	0.02	1.33	7.71	0.04	0.03	33.29	3.72	0.98	0.88	0.91
Shb-11	2.50	3.07	1.23	−29.5	47.68	8.93	6.85	1.58	0.92	0.39	0.23	0.27	0.21	0.02	1.30	7.52	0.04	0.03	32.62	3.36	0.98	0.88	0.91
Shb-12	3.65	3.38	0.93	−29.6	50.69	6.55	6.3	1.05	0.91	0.34	0.17	0.21	0.19	0.02	1.04	5.53	0.03	0.03	33.16	2.70	0.98	0.87	0.92
Shb-13	6.52	3.14	0.48	−30.5	49.79	6.43	6.28	1.05	0.9	0.32	0.17	0.2	0.19	0.02	1.02	5.53	0.03	0.03	33.05	2.71	0.98	0.87	0.92
Shb-14	12.30	4.59	0.37	−30.1	42.78	13.25	8.03	1.47	1.02	0.32	0.26	0.36	0.28	0.03	1.65	5.25	0.04	0.03	28.68	3.24	0.98	0.89	0.92
Shb-15	1.50	2.80	1.87	−30.0	42.76	13.38	8.06	1.48	0.98	0.32	0.25	0.39	0.28	0.02	1.66	5.29	0.05	0.03	28.79	3.10	0.98	0.89	0.92
max	12.30	4.59	1.98	−28.90	52.18	13.38	8.06	1.95	1.02	0.52	1.35	0.39	0.28	0.03	1.66	6.96	0.05	0.04	41.08	25.14	0.99	0.89	0.93
min	1.20	2.09	0.36	−31.40	35.76	6.43	5.34	1.02	0.63	0.25	0.15	0.20	0.13	0.02	1.02	7.85	0.04	0.02	27.36	2.13	0.97	0.87	0.87
avg	4.91	3.25	1.10	−30.25	45.10	9.35	6.91	1.47	0.90	0.35	0.41	0.29	0.22	0.02	1.33	6.68	0.04	0.03	32.12	6.82	0.98	0.88	0.91

[a]TOC: Total organic carbon, wt %. TS: Total sulfur, wt %. CIA: Chemical index of alteration [CIA = Al/(Al + K + Na).

https://doi.org/10.1021/acsomega.4c02582
ACS Omega 2024, 9, 27458−27479

http://pubs.acs.org/journal/acsodf

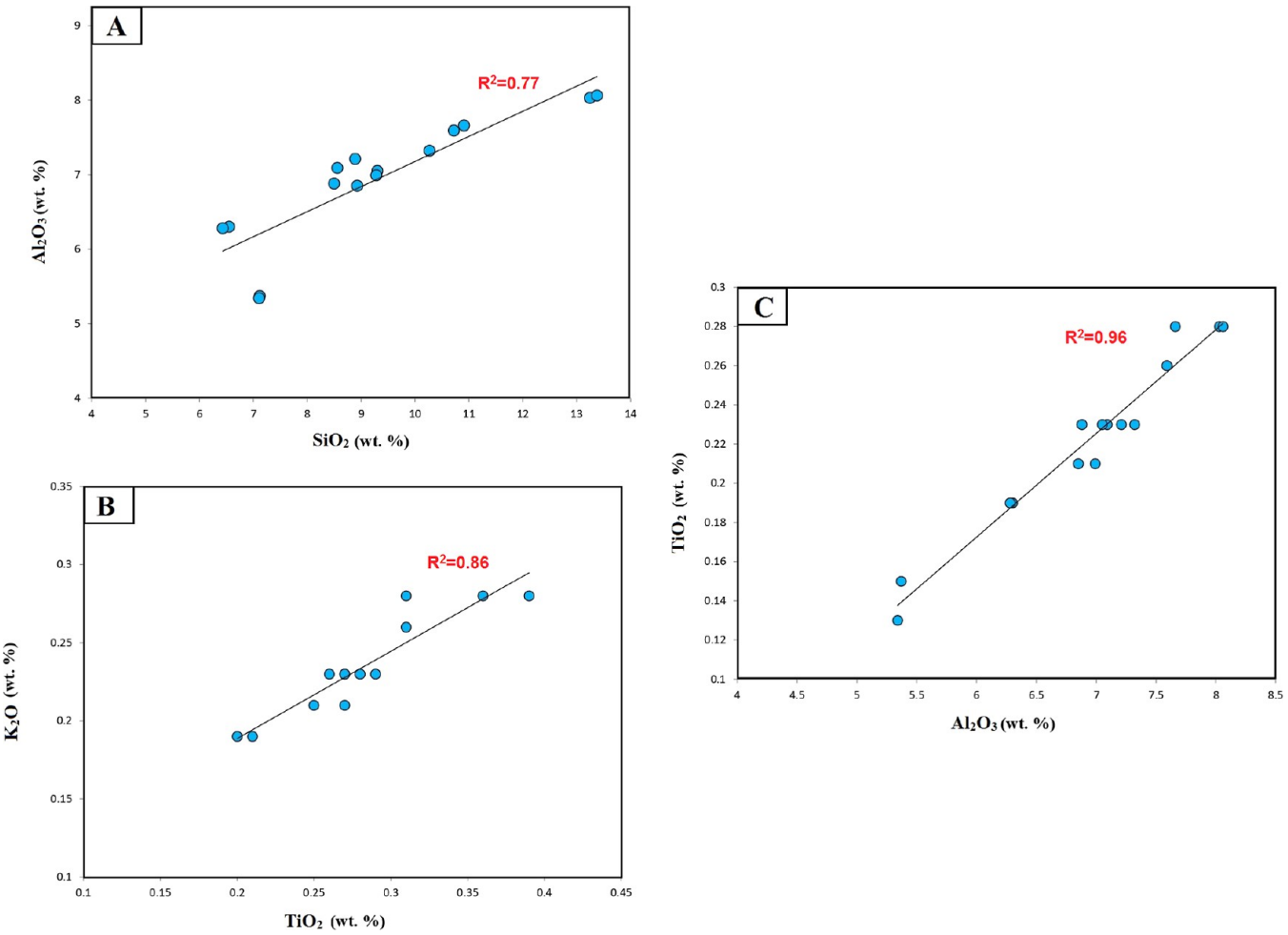

Figure 5. (A) Relationship between SiO_2 and Al_2O_3 contents and (B,C) relationships between TiO_2 and (B) K_2O and (C) Al_2O_3K contents in the studied carbonate-rich samples, showing that the Si and Ti elements are mainly sourced from clay minerals.

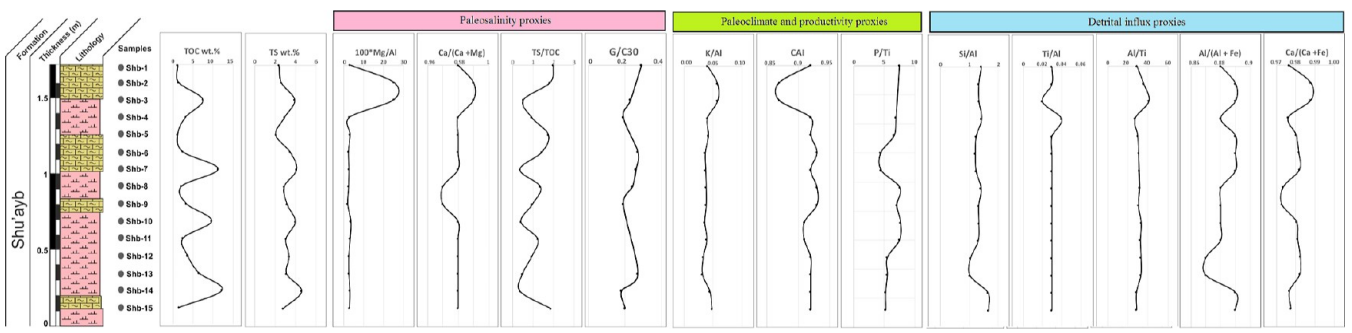

Figure 6. Chemostratigraphy distribution of TOC, TS, and geochemical ratios of Si/Al, P/Ti, K/Al, Ti/Al, Al/Ti, 100 × Mg/Al, Ca/(Ca + Fe), Al/(Al + Fe), and CIA for the Upper Cretaceous Shu'ayb Formation from the Ajloun outcrop in Northern Jordan.

K_2O together with TiO_2, as indicated by the adjusted R^2 values of 0.75 and 0.85 (Figure 5B,C). These correlations suggest the existence of Ti within clay lattices and low detrital input.[39]

Furthermore, different salinity, climate, paleoproductivity, and detrital influx proxies were estimated depending on the amounts of their major elements. These geochemical ratios are Si/Al, P/Ti, K/Al, Ti/Al, Al/Ti, Ca/Ca + Fe, Al/Al + Fe, and the chemical index of alteration (CIA) value, which were found to be in the range of 1.02−1.66, 6.96−7.85, 0.04−0.05, 0.02−0.04, 27.36−41.08, 0.87−0.89, 0.97−0.99, 0.87−0.89, and 0.87−0.93, respectively (Table 1). These ratios of salinity, paleoclimate, detrital influx, and water depth of the depositional environment setting are markedly similar to each other and to the TOC profile (Figure 6).

4.5. Hydrocarbon and Biomarker Distributions. Hydrocarbon distributions of some saturated HC fractions of OM in samples such as normal alkane, acyclic isoprenoid, terpane, and sterane biomarkers were determined using the mass fragmentogram on m/z 85, 191, and 217 ions in GC−MS.

n-Alkane and acyclic isoprenoid distributions show that most of the studied samples display a bimodal distribution along the entire C_{15}−C_{34} range (Figure 7). This hydrocarbon distribution

https://doi.org/10.1021/acsomega.4c02582
ACS Omega 2024, 9, 27458−27479

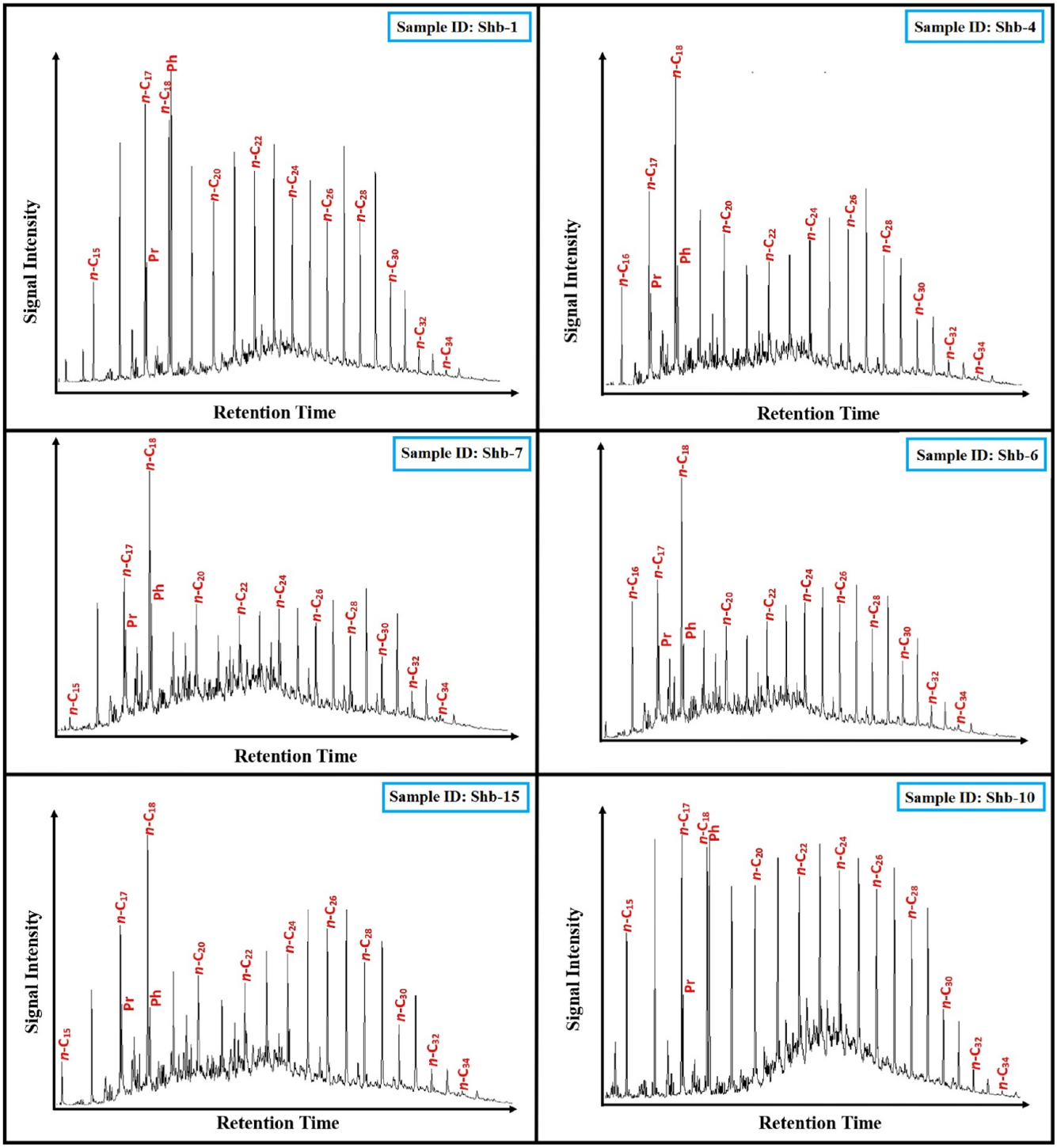

Figure 7. *m*/*z* 85 mass fragmentograms showing *n*-alkane and acyclic isoprenoid (e.g., pristane and phytane) distributions of the aliphatic fraction in the extracted bitumen from the studied bituminous carbonate rock in the Ajloun area.

of the studied samples result in carbon preference index (CPI) and waxiness index (WI) in the range of 1.01−1.41 and 1.05−1.38, respectively, as shown in Table 2.

In addition, the chromatograms show that isoprenoid hydrocarbons (Pr and Ph) predominate, aside from *n*-alkanes (Figure 7). These acyclic isoprenoids and their relative ratios (Pr/Ph, Pr/*n*-C_{17}, and Ph/*n*-C_{18}) are widely used to understand the paleo-redox conditions.[40,41] However, Ph generally predominated over Pr in most of the chromatograms (Figure 7), resulting in a low Pr/Ph ratio of the majority of the studied samples between 0.39 and 0.97 (Table 2). Moreover, the isoprenoid ratios were also found based on the proportion of *n*-C_{17} and *n*-C_{17} over Pr and Ph, with ratios from 0.40 to 0.62 and from 0.33 to 1.13, respectively (Table 2).

A considerable number of hopanes, including C_{30} hopanes, C_{29} norhopanes, and homohopanes of C_{31}−C_{35}, were detected using *m*/*z* 191 mass fragmentograms (Figure 8A). They clearly show that the frequency of C_{30} hopanes is relatively more than that of C_{29} norhopanes (Figure 8A), resulting in relatively high C_{29}/C_{30} hopane values of 0.54−1.05 (Table 2). C_{31} hopane is

https://doi.org/10.1021/acsomega.4c02582
ACS Omega 2024, 9, 27458−27479

Table 2. Different Biomarker Ratios of the Bituminous Carbonate Rock throughout the Upper Cretaceous Shu'ayb Formation from the Ajloun Outcrop, Illustrating Source Organic Matter Input and Depositional Environment Conditions[a]

samples depth (m)	normal alkanes and isoprenoids					triterpanes and terpanes (m/z 191)							steranes (m/z 217)				dibenzothiophene and phenanthrene m/z 78 and 84
	Pr/Ph	Pr/C_{17}	Ph/C_{18}	WI	CPI	hopanes				tricyclic terpanes			C_{29}/C_{27} regularsteranes	regular steranes (%)			
						C_{29}/C_{30}	G/C_{30}	HCR_{31}/HC_{30}	HC_{35}/HC_{34}	C_{26T}/C_{25T}	C_{23T}/C_{24T}	C_{24Te}/C_{24T}		C_{27}	C_{28}	C_{29}	DBT/Phen
Shb-1	0.39	0.40	1.04	1.10	1.22	0.54	0.29	0.66	1.54	0.67	2.62	0.87	0.61	47.35	23.90	28.75	1.83
Shb-3	0.56	0.45	0.86	1.14	1.13	0.59	0.23	0.61	1.38	0.61	2.90	0.85	0.78	44.94	20.00	35.06	1.54
Shb-4	0.97	0.49	0.34	1.38	1.26	0.82	0.19	0.43	1.52	0.62	2.28	0.92	0.90	40.37	23.11	36.53	1.65
Shb-6	0.90	0.52	0.33	1.21	1.09	0.93	0.27	0.40	1.34	0.74	1.90	0.80	0.89	39.62	24.94	35.44	1.50
Shb-7	0.81	0.62	0.44	1.05	1.32	0.86	0.26	0.33	1.75	0.47	2.99	0.90	0.66	46.78	22.30	30.92	2.17
Shb-9	0.74	0.43	0.37	1.18	1.19	0.92	0.24	0.39	2.50	0.56	1.82	0.86	1.20	35.90	20.85	43.25	1.09
Shb-10	0.44	0.47	1.13	1.05	1.41	1.05	0.19	0.32	1.76	0.50	1.89	0.62	0.69	35.78	39.45	24.77	2.50
Shb-13	0.65	0.45	0.70	1.12	1.01	1.03	0.27	0.25	2.00	0.66	2.84	0.80	0.51	52.51	20.46	27.03	1.65
Shb-14	0.78	0.55	0.47	1.15	1.10	0.95	0.18	0.38	1.48	0.76	2.18	0.84	0.74	45.33	21.23	33.44	1.23
Shb-15	0.88	0.56	0.37	1.20	1.14	0.89	0.20	0.32	1.89	0.65	2.23	0.84	0.59	48.34	23.10	28.56	1.55
maximum	0.97	0.62	1.13	1.38	1.41	1.05	0.29	0.66	2.50	0.76	2.99	0.92	1.20	52.51	39.45	43.25	2.50
minimum	0.39	0.40	0.33	1.05	1.01	0.54	0.18	0.25	1.34	0.47	1.82	0.62	0.51	35.78	20.00	24.77	1.09
average	0.71	0.50	0.63	1.17	1.19	0.85	0.23	0.42	1.75	0.62	2.37	0.82	0.78	43.77	24.90	32.65	1.69

[a]Pr—Pristane, Ph—phytane, CPI—carbon preference index = $\{2(C_{23} + C_{25} + C_{27} + C_{29})/(C_{22} + 2[C_{24} + C_{26} + C_{28}] + C_{30})\}$, waxiness index (WI) = Σ (n-C21- n-C31)/Σ (n-C15- n-C20), HCR_{31}/HC_{30}: C_{31} regular homohopane/C_{30} hopane, C_{29}/C_{30}: C_{29} norhopane/C_{30} hopane, G/HC_{30} = gammacerane/C_{30} hopane, DB = dibenzothiophene, Phen = phenanthrene.

https://doi.org/10.1021/acsomega.4c02582
ACS Omega 2024, 9, 27458−27479

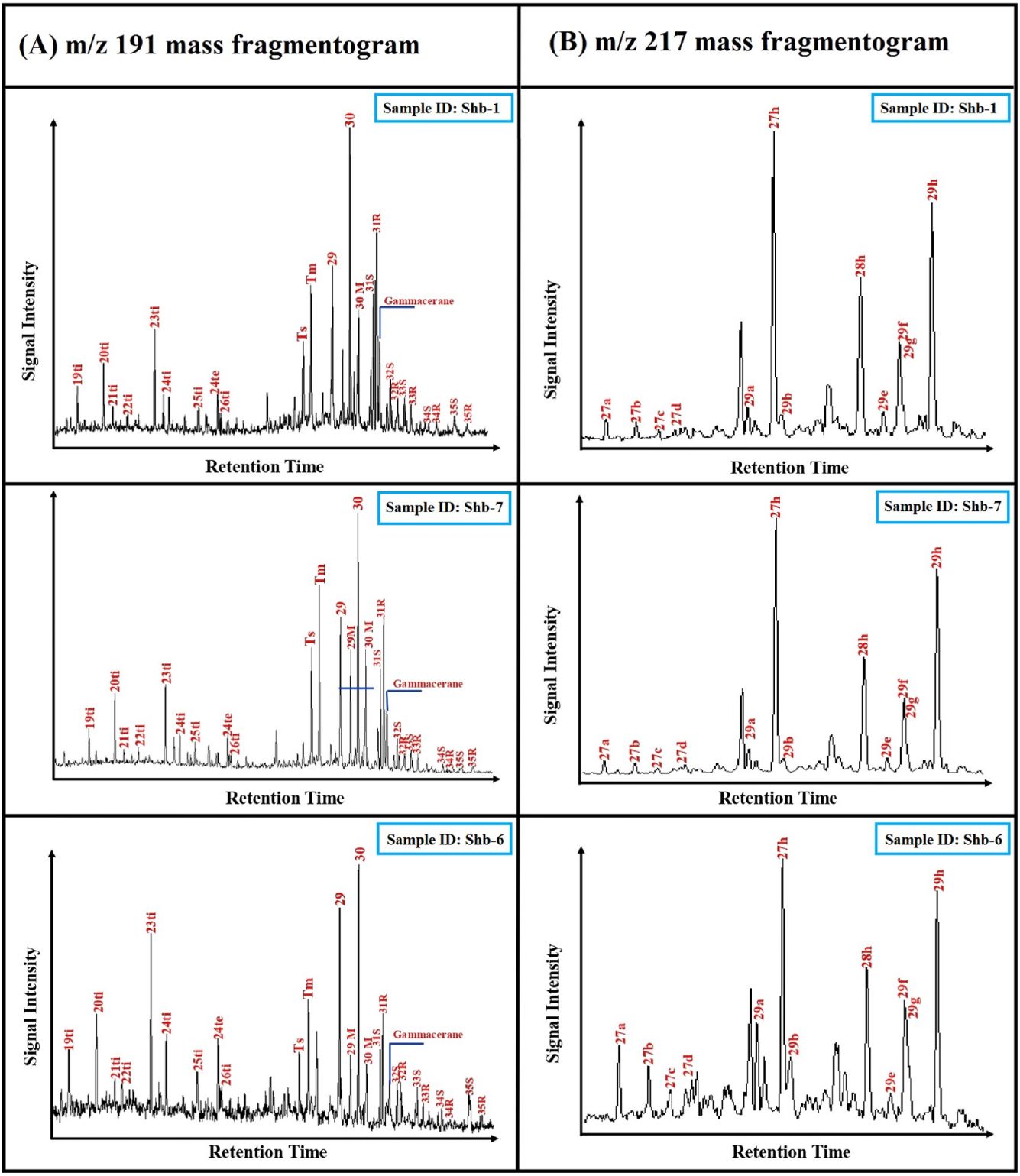

Figure 8. *m*/z 191 and 217 mass fragmentograms of the aliphatic fraction in the extracted bitumen from the studied bituminous carbonate rock in the Ajloun area.

also dominant when compared with the composition of homohopane series (Figure 8A). However, the frequency of C_{30} hopanes is also more than C_{31R} homohopane and gammacerane (Figure 8A), resulting in lower $C_{31}R/C_{30}H$ (0.25−0.55) and G/C_{30} (0.14−0.29) ratios (Table 2).

In addition, the *m*/*z* 191 data displayed high numbers of tricyclic terpanes, ranging from C_{19} to C_{26} (Figure 8A). Tricyclic terpanes were identified by the significant numbers of C_{19}, C_{20}, and C_{23} tricyclic terpanes (Figure 8A). The proportion of C_{23}tri/C_{24}tri was found to be more than 1.8 (Table 2). Additionally, several tricyclic terpane ratios such as C_{24}Te/C_{24}T and C_{26}T/C_{25}T were calculated and used to infer about the depositional environment setting, as discussed in the next subsections.

https://doi.org/10.1021/acsomega.4c02582
ACS Omega 2024, 9, 27458−27479

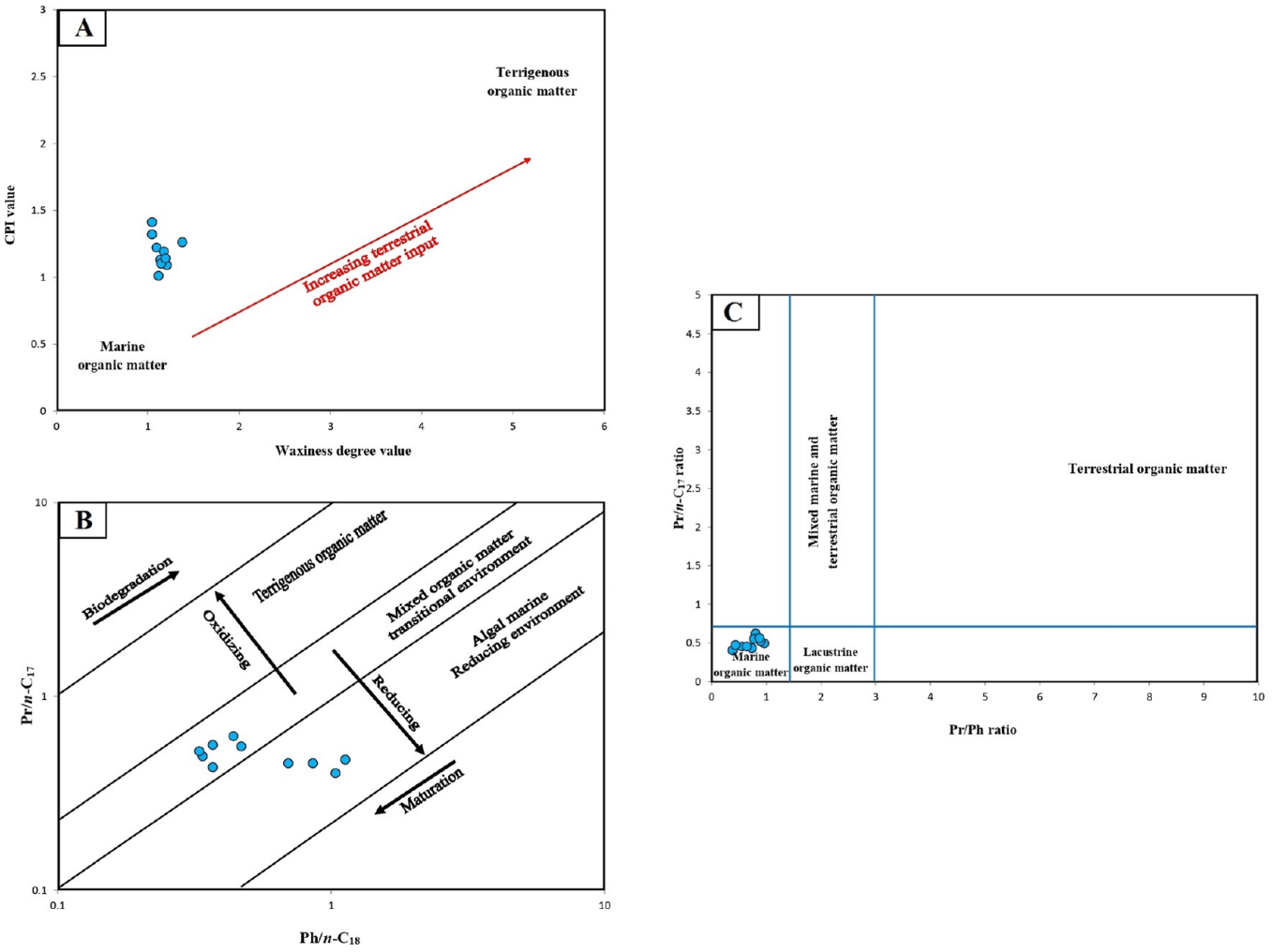

Figure 9. Geochemical biomarker results of the extracted bitumen from the studied bituminous carbonate rock in the Ajloun area, showing (A) CPI versus waxiness degree and (B) pristane/n-C_{17} versus phytane/n-C_{18}, and (C) pristane/n-C_{17} Pr/Ph, indicating that these bituminous carbonate sediments contain mainly marine OM and deposited under anoxic environmental conditions.

Steranes and diastereomers were produced by the m/z 217 mass fragmentogram of the studied extracted samples (Figure 8B). Results showed that there was a significant abundance of steranes (Figure 8B). The distribution of C_{27}−C_{29} regular steranes represented by a majority of C_{27} regular sterane, with a minority of and C_{29} and C_{28} regular steranes (Figure 8B), which provided ratios of 35.78−52.51% for C_{27}, 27.77−43.25% for C_{29}, and 20.00−39.45% for C_{28} and a high C_{27}/C_{29} regular ratio between 0.83 and 1.94 (for more information, see Table 2).

In addition, polycyclic aromatic hydrocarbons like dibenzothiophene (DBT) and phenanthrene (P) were recognized in the unsaturated fractions of the studied samples using m/z 178 and m/z 184 ions. The DBT/P ratio was calculated based on the relative abundance of DBF and P and is a useful indicator of depositional environment and lithologies.[42,43] In this case, the samples have a high DBT/P ratio of more than 1, ranging from 1.09 to 2.50, as shown in Table 2.

5. DISCUSSION

5.1. Origin and Source of Organic Matter Input. Knowledge on the origin and source of OM input to the bituminous carbonate rocks of the Shu'ayb Formation was primarily obtained by employing multibiomarker proxies together with kerogen microscopy.

The saturated and heterocyclic aromatic hydrocarbons, supported by their ratios, provided important information for assessing the OM input during the accumulation. As a result, the bimodal distributions of hydrocarbon in the studied samples revealed multisource OM with a substantial input of the marine one.[44,45] This deduction was further strengthened by the plot of CPI vs WI (Figure 9A). Moreover, verification of the significant influx of algal marine-derived OM into the Shu'ayb bituminous carbonate rocks was done by analyzing the isoprenoids and their ratios (Figure 9B,C).

Further, the understanding of the OM input was gained by cross-verifying and utilizing hopane and terpane biomarkers (Figure 8A), along with their ratios (Table 2). In this case, the majority of the studied samples exhibited a $C_{31}R/C_{30}$ hopane ratio of greater than 0.25 (Table 2), suggesting the origin from marine source rocks.[46,47] This observation was supported by the correlation between the high $C_{31}R/C_{30}$ hopane ratio and the low C_{26T}/C_{25T} ratio of less than 1 (Figure 10A). The higher DPT/P ratio consistently more than 1 in the majority of the examined samples is a suggestive indication of the marine origin of OM input (Figure 10B).

The marine contribution of OM was further supported by the distribution of tricyclic terpanes and their ratios, as detailed in Table 2. The high occurrences of C_{23} tricyclic and relatively high

https://doi.org/10.1021/acsomega.4c02582
ACS Omega 2024, 9, 27458−27479

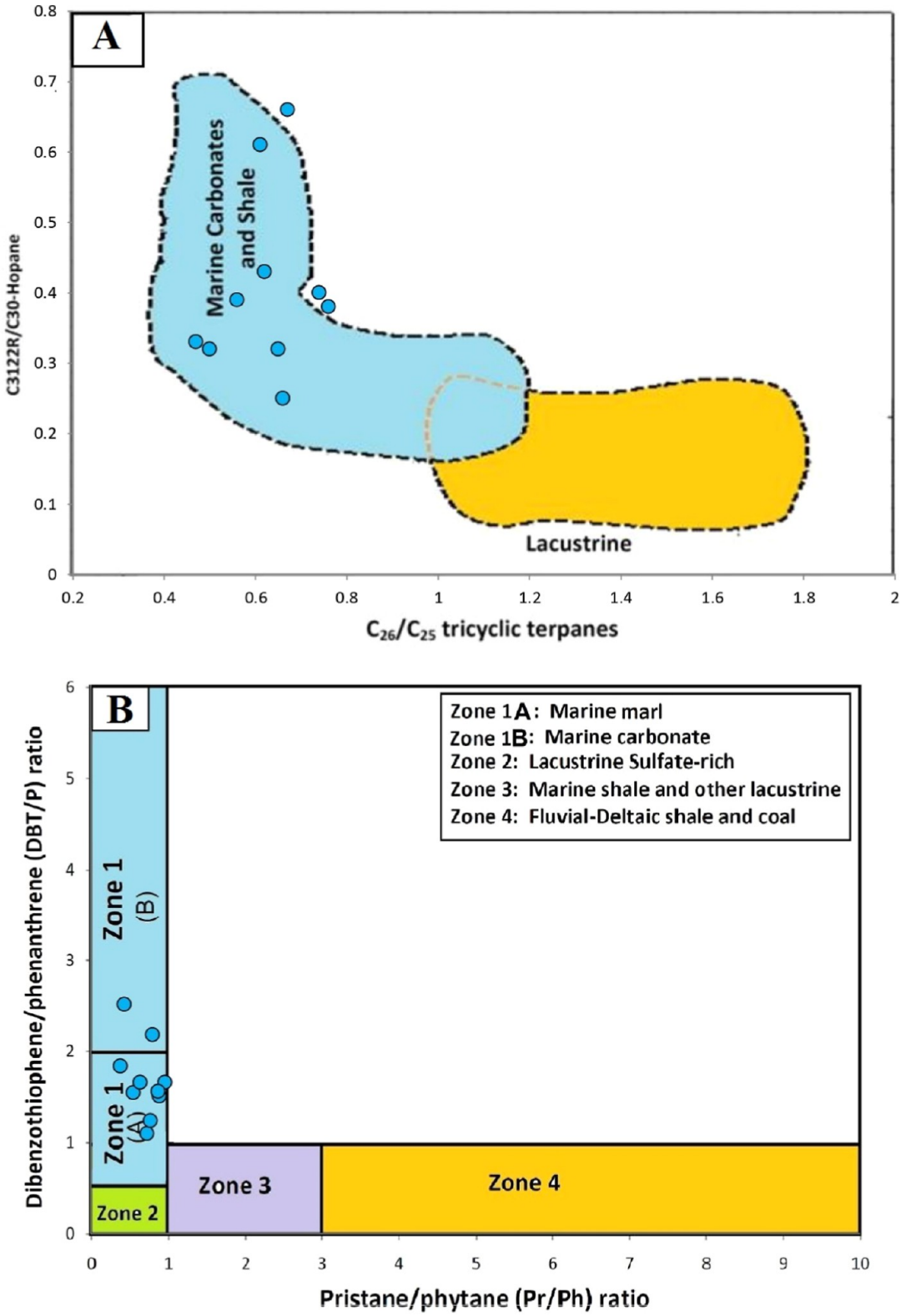

Figure 10. Geochemical biomarker results of the extracted bitumen from the studied bituminous carbonate rock in the Ajloun area, showing (A) CR_{31}/C_{30} homohopane versus C_{26}/C_{25} tricyclic terpane ratio and (B) Pr/Ph versus DBT/P, indicating marine carbonate-rich facies.

C_{24} tricyclic-to-C_{24} tetracyclic terpane ratio (Figure 8A), associated with the C_{23}triT/C_{24}T ratio which exceeds 2 and the C_{24}te/C_{24}T ratio of less than 1 (Table 2), suggesting a tremendous evolution of marine OM into the Shu'ayb bituminous carbonate strata (Figure 11A).

In terms of regular steranes, the examined oil shales showed higher values of C_{27} over C_{29}, with a substantial C_{27}/C_{29} ratio exceeding 1 (Table 2). This elevated ratio supports the presence of marine OM, especially with significant input from algae (Figure 11B). The interpretation was further supported by the distribution pattern of C_{27} to C_{29} regular steranes, indicating that

https://doi.org/10.1021/acsomega.4c02582
ACS Omega 2024, 9, 27458−27479

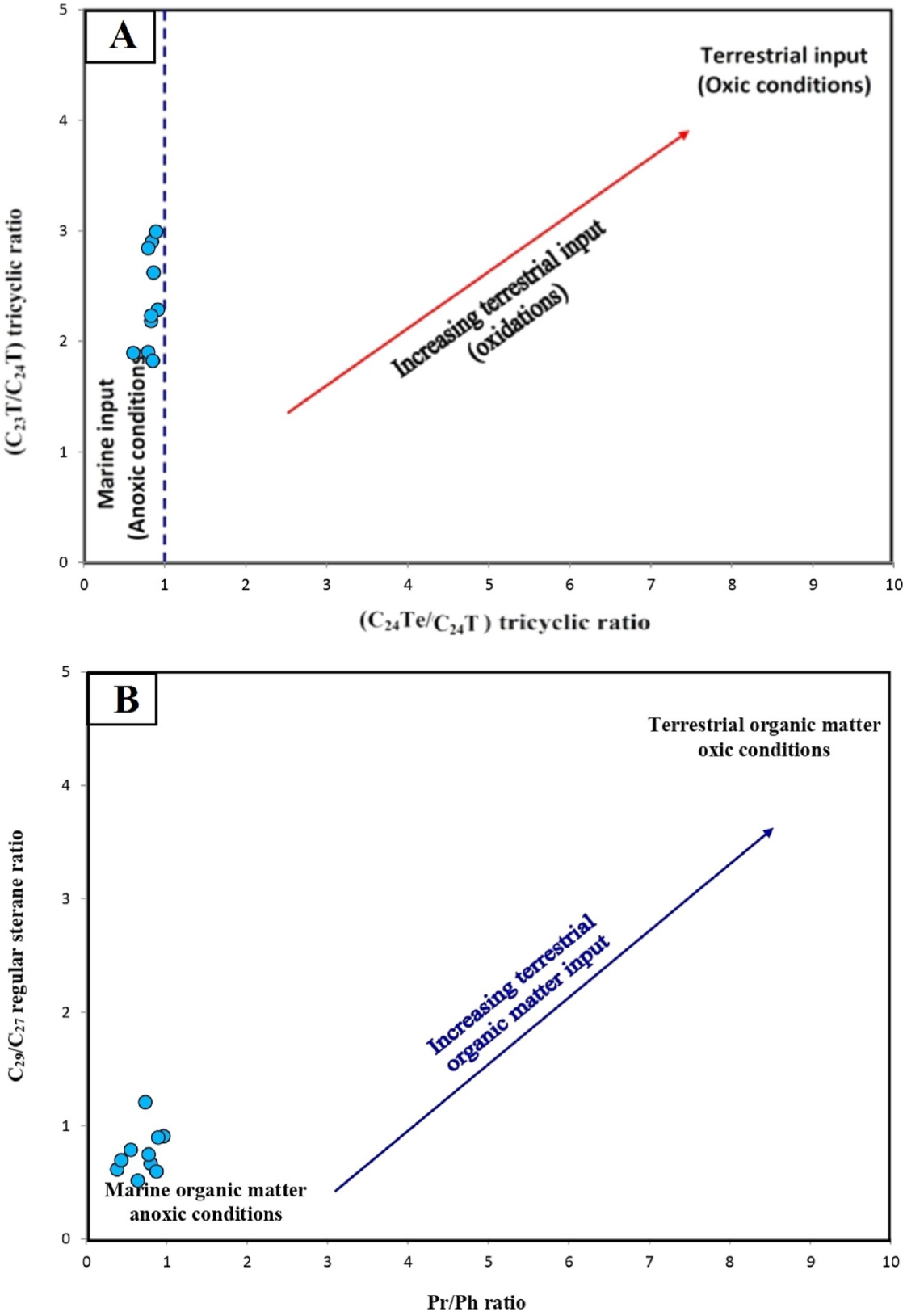

Figure 11. Geochemical biomarker results of the extracted bitumen from the studied bituminous carbonate rock in the Ajloun area, showing (A) $C_{23T}/_{24T}$ versus C_{24Te}/C_{24T} and (B) Pr/Ph versus C_{29}/C_{27} regular sterane, indicating that marine OM was deposited under anoxic conditions.

OM primarily derived from planktonic zoophyte and algal origins, with little input of OM derived from terrestrial materials based on the diagram provided by Huang and Meinschein,[48] as shown in Figure 12.

In addition, the high occurrences of phytoplankton algae (i.e., lamalginite assemblages; Figure 3A–F) in the studied samples also worked well with the biomarker results. The lamalginite

https://doi.org/10.1021/acsomega.4c02582
ACS Omega 2024, 9, 27458−27479

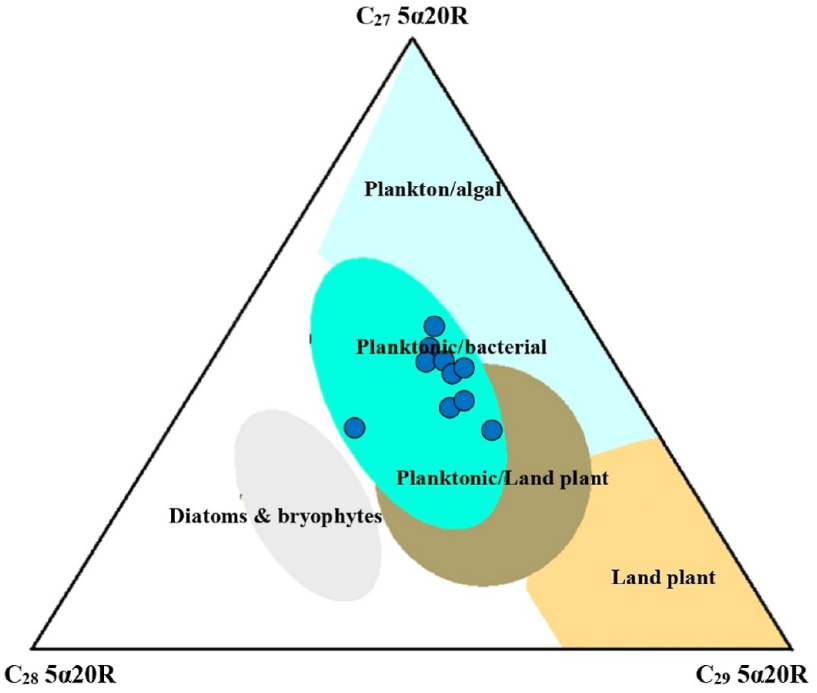

Figure 12. Ternary diagram of regular steranes (C_{27}, C_{28} and C_{29}) of the extracted bitumen from the studied bituminous carbonate rock in the Ajloun area, showing the relationship between the sterane compositions and the OM input. .

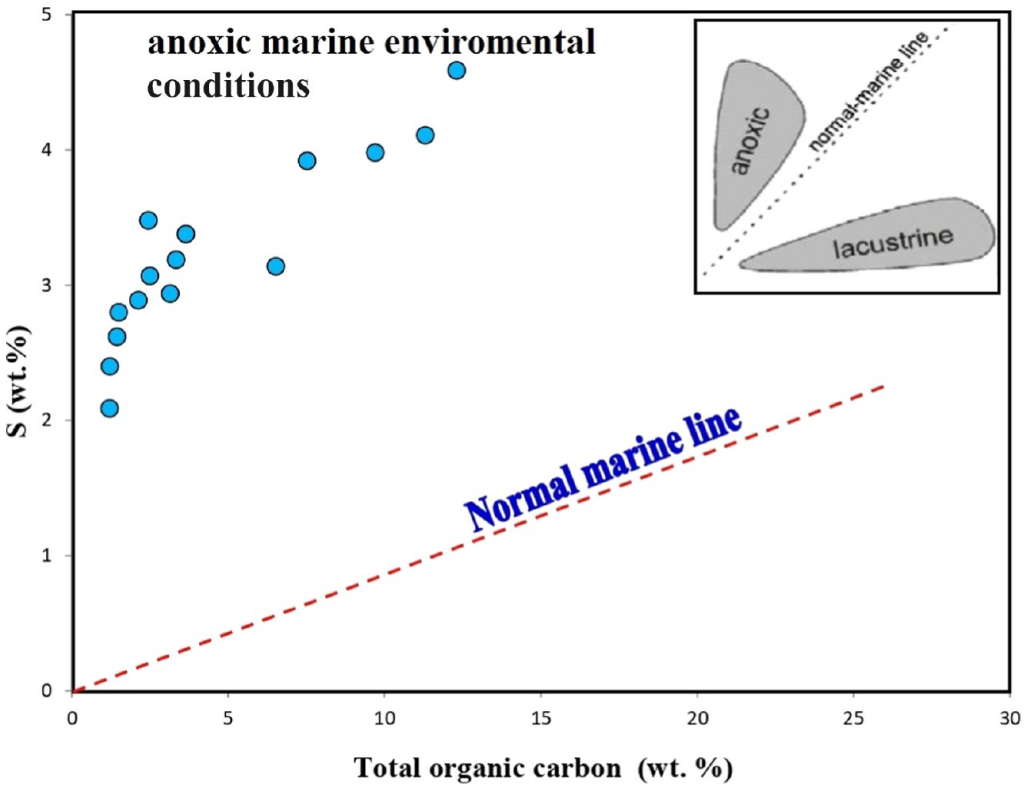

Figure 13. Relationship between TOC and TS contents for the studied bituminous carbonate rock in the Ajloun area, showing an anoxic marine environmental setting.

algae assemblages are considered to be of marine origin and were deposited under redox conditions.[30,31]

5.2. Paleoredox Conditions. The paleoredox conditions are an important factor and majorly impact the preservation of OM,[47,48] where four conditions can be distinguished based on the availability of O_2 in bottom water, namely, oxic, dysoxic, anoxic nonsulfidic, and anoxic sulfidic (euxinic) conditions.

Anoxic condition was recognized during the deposition time of Shu'ayb Formation based on the high values of OM in the bituminous carbonate succession, where the TOC reached up to 12.30 wt % (Table 1), which, in turn, enhanced the preservation

https://doi.org/10.1021/acsomega.4c02582
ACS Omega 2024, 9, 27458−27479

and organic enrichment. Moreover, the high OM is mainly associated with high total sulfur (TS) content, which is considered as a better proxy for the reducing marine environment than the pyritic sulfur in sediments.[17,32] In this case, highly reducing marine environmental conditions showed a high S value which exceeds 2 wt %,[17] which has been seen in the studied bituminous carbonate samples, as characterized by a high TS content of up to 4.59 wt % (Table 1). The explanation of highly reducing marine environmental conditions was clearly demonstrated by the association between the TOC and S of the samples (Figure 13). Moreover, the concentrations of TOC and S contents together with Fe element were plotted on the Fe−TOC−S ternary diagram of Dean and Arthur[49] and show that most of the analyzed Shu'ayb bituminous carbonate samples plotted on the zone of high Fe sulfurized during the poor-oxygenated environments, with a S/Fe ratio of more than 1.5 (Figure 14).

In addition, the redox conditions (i.e., reduction vs oxidation) during the time of deposition were also assessed using the isoprenoid biomarker and its Pr/Ph ratio.[40,50] For example, Pr/Ph < 1 suggests an anoxic condition in a calm and quiet environment, and Pr/Ph of >2 points to terrestrial influences and translates to an oxic condition.[51] In this study, the Shu'ayb bituminous carbonate sediments were accumulated during anoxic depositional settings, as deduced by a narrow Pr/Ph ratio (0.39 to 0.97) (Table 2), as anoxic conditions endorse Ph occurrences over Pr.[52] The high Ph/n-C_{18} ratio also agreed with the redox (anoxic) conditions during the accumulation of carbonate sediments, as shown in Figure 9B.

The marine anoxic conditions in the Shu'ayb bituminous carbonate sediments were also indicated by the distribution of homohopanes, whereby the C_{35} homohopanes dominated relative to the C_{34} homohopanes, with C_{35}/C_{34} ratios having the highest values between 1.34 and 3.5 (Table 2).

5.3. Paleosalinity Conditions. The paleosalinity condition is important and helpful for recognizing how organic carbon is enriched, as assessed from the biological evidence and anoxic conditions of the water column.[53]

In this study, major elements that indicate the salinity of the studied samples, including Ca, Mg, Fe, and Al elements, and their 100 × Mg/Al, Ca/Mg, and Ca/Ca + F indexes (Table 1) were used to estimate the salinity degree during the deposition.[54−56]

The value of less than one for the ratio 100 × Mg/Al index infers freshwater conditions, while above five of the same ratio suggests the salinity water conditions.[54,55] Accordingly, the studied bituminous carbonate rocks of the Shu'ayb Formation were deposited in salinity water, with an average value of 6.82 of 100 × Mg/Al index (Table 1). This interpretation of the salinity water conditions was confirmed by the relationship between the 100 × Mg/Al index and the high Ca/Mg ratio (Figure 15). Additionally, the proportion of inorganic elements, i.e., Ca and Fe and their Ca/Ca + Fe ratios also provide salinity inferences.[57,58] In this regard, saline water showed a high Ca/Ca + Fe ratio of more than 0.8, while the Ca/Ca + Fe ratio between 0.4 and 0.8 indicated brackish water, and a value of <0.4 was indicative of freshwater during deposition.[57,58] The studied Shu'ayb bituminous carbonate rocks exhibited a Ca/Ca + Fe ratio >0.8 (0.97−0.99; Table 1), corresponding to the saline water.

Additionally, the proportion of TOC and TS contents and their S/TOC ratio also provide salinity inferences.[33] Wei and Algeo[33] reported that the calculated S/TOC ratio of a range

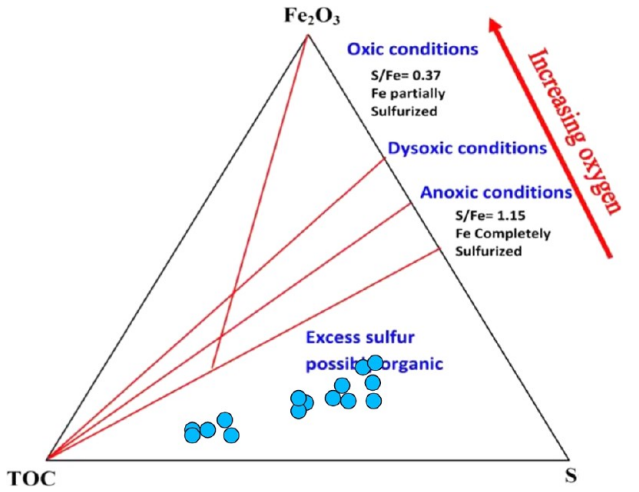

Figure 14. Fe−TOC−S ternary diagram of carbonate samples of the Shu'ayb Formation, showing low oxygen content (anoxic conditions) during deposition (modified after Dean and Arthur[49]).

between 0.01 and 0.06 indicates freshwater environments, while the S/TOC ratio with values ranging between 0.07 and 0.35 is associated with deposition in a brackish-water environment, and the sediments deposited in a marine environment have a relatively high S/TOC ratio in the range of 0.17−0.47. Looking at the environmental salinity characteristics based on the S/TOC ratio above and comparing it with that of the studied Shu'ayb bituminous carbonate facies, it shows that most of the Shu'ayb carbonate samples fall within the marine (seawater) environment, with a high S/TOC ratio between 0.36 and 1.98 (Table 1).

One of the prominent features of the salinity stratification of the water column is the occurrence of gammacerane in the m/z 191 mass fragmentogram (Figure 8A). The high gammacerane/C_{30} hopane (G/C_{30}) ratio is linked with stratification (hypersalinity) conditions of the water columns.[59]

The moderate gammacerane index of the samples (0.14 and 0.29) (Table 2) corresponds to moderate stratification during deposition of the Shu'ayb bituminous carbonate rocks. This finding is consistent with the Pr/Ph and C_{35}/C_{34} ratios versus G/C_{30} ratio (Figure 16), as the layering, in effect of salinity, of the water columns regulates the oxygen content during the accumulation the bituminous carbonate sediments of the Shu'ayb Formation.[53]

5.4. Paleoclimate Conditions and Paleoproductivity. The paleoclimate conditions were reconstructed based on multiple proxies, including inorganic geochemical data together with foraminifera assemblages, as presented in the previous subsections.

The major oxides like, SiO_2, Al_2O_3, K_2O, and Na_2O (Table 1), can be obtained to reveal warm and humid climates.[17,60,61] However, Al_2O_3 and K_2O are major oxides, and their K/Al ratio is widely accepted to investigate the paleoclimatic conditions.[61−63] Al generally occurs within the kaolinite and are known to be linked with a warm climate,[64,65] while K can be found within the illite and reflecting dry and cold climatic conditions.[66] In this case, lower K/Al ratios are extensively related to hot and humid climatic conditions, wherein there is enhanced contribution of kaolinite and to a lesser extent illite.[62,63,67] The K/Al ratio for most of the studied carbonates reveals lower values in the range 0.04 to 0.05 (Table 1),

https://doi.org/10.1021/acsomega.4c02582
ACS Omega 2024, 9, 27458−27479

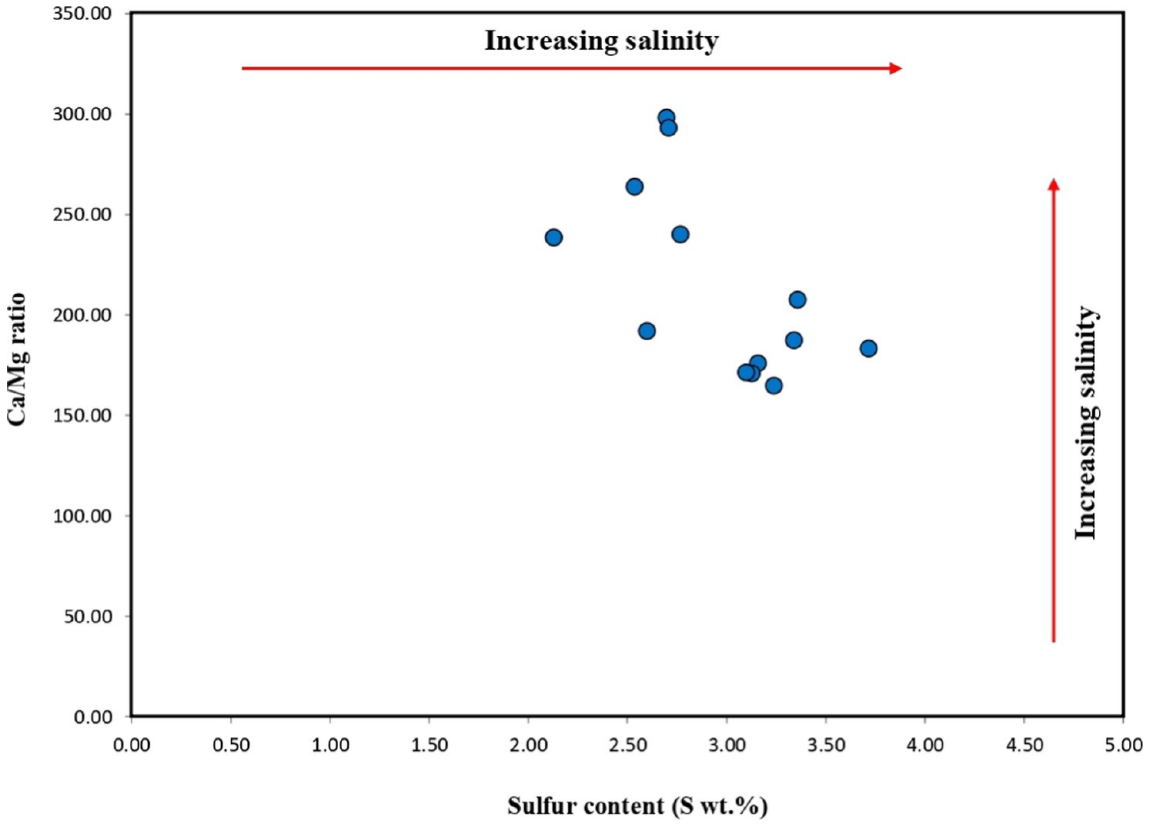

Figure 15. Ca/Mg vs 100 × Mg/Al ratio plot, showing salinity seawater during the deposition time of the studied bituminous carbonate rock from the Shu'ayb Formation in the Ajloun area, Northern Jordan.

suggesting higher kaolinite than illite contents and the presence of warm and humid climatic conditions.

However, the chemical index of alteration [CIA = Al/(Al + Na + K)] was calculated based on the formula of Nesbitt and Young[68] and also used to assess the amount of weathering of pre-existing rocks, which can provide clues about the climatic conditions.[60,70−73] CIA values of 0.8−1.0 are extensively related to hot and humid climatic conditions. While cold and arid climatic conditions are associated with lower CIA values of less than 0.7.[68−71] The results show that the CIA for most of the studied carbonates reveal values in the range 0.87 to 0.93 (Table 1), suggesting that a warm and humid climate prevailed during the period of organic-rich carbonate deposition. This interpretation of the warm-humid climatic conditions is also consistent with the high abundance of OM/phytoplankton and algal origin, together with foraminifera assemblages, as observed via microscopic examinations (Figures 4 and 5) and biomarker distributions of isoprenoids (Figure 9B) and regular steranes (Figure 12).

However, most of the modern analogues are warm water provinces.[66] Many planktonic foraminifera can be indicators of these warming, as temperature controls its composition, shell size, and its diversity to a certain extent.[72−74] The most species that are preferred for warming are *Globigerina* sp., *Globorotalia* sp., *Globigerinoides* sp., *Globoturborotaliid* sp., and *Orbulina* sp.[75] The studied Shu'ayb carbonate facies have mainly *Globigerinoides* sp. and *Orbulina* sp. (Figure 4), suggesting the plankton fauna in these carbonate sediments is typical of warm-water conditions.

In this case, we believed that the presence of a warm and humid climate therefore enhanced increasing in the nutrient level on the sea surface and appearance of some high nutrient indicator species. However, most of the nutrients are phosphorus (P) and nitrogen (N), which commonly occur in seawater. Higher P concentrations in the seawater enhance the growth of algae and cause large phytoplankton blooms. Particularly, Shu'ayb samples consist of a high abundance of P oxide, with a range between 1.04 and 1.95 wt % (Table 1), which is considered to be much higher than the average for shale (0.19 wt %).[8] However, the P element is mainly dissolved in OM or absorbed on the sediments' surface areas. In this regard, the weak correlation between P_2O_5 (%) and Ti (ppm) in the Shu'ayb carbonate samples of this study (Figure 17) indicates that P is of organic origin and can be used as a paleoproductivity proxy.[78] In this context, the relationship between P and Ti elements and their P/Ti ratio can be used as a proxy to indicate the role of marine primary productivity during deposition.[76,77] For example, a P/Ti ratio <0.34 reveals low paleo-productivity; 0.34 < P/Ti < 0.79 and P/Ti > 0.79 are associated with medium to high paleoproductivities.[76] In this point of view, most of the studied Shu'ayb carbonate samples are characterized by high marine primary productivity, as indicated by the P/Ti ratios of more than 6 (Table 1).

5.5. Detrital Influx and Water Depth. The chemical composition of sediment fractions is reflected by the accumulated siliciclastic and carbonate mineral-associated elements.[78] Aluminum (Al_2O_3), titanium (TiO_3), silicon (SiO_2), sodium (NaO), and magnesium (MgO) are associated with minerals derived from the land such as quartz and clays[79,80] and frequently used to estimate the detrital influx.[81,82] For example, the relative abundance of Si, and thus Si/Al, in a predominantly detrital interval can be used as a reliable proxy for

https://doi.org/10.1021/acsomega.4c02582
ACS Omega 2024, 9, 27458−27479

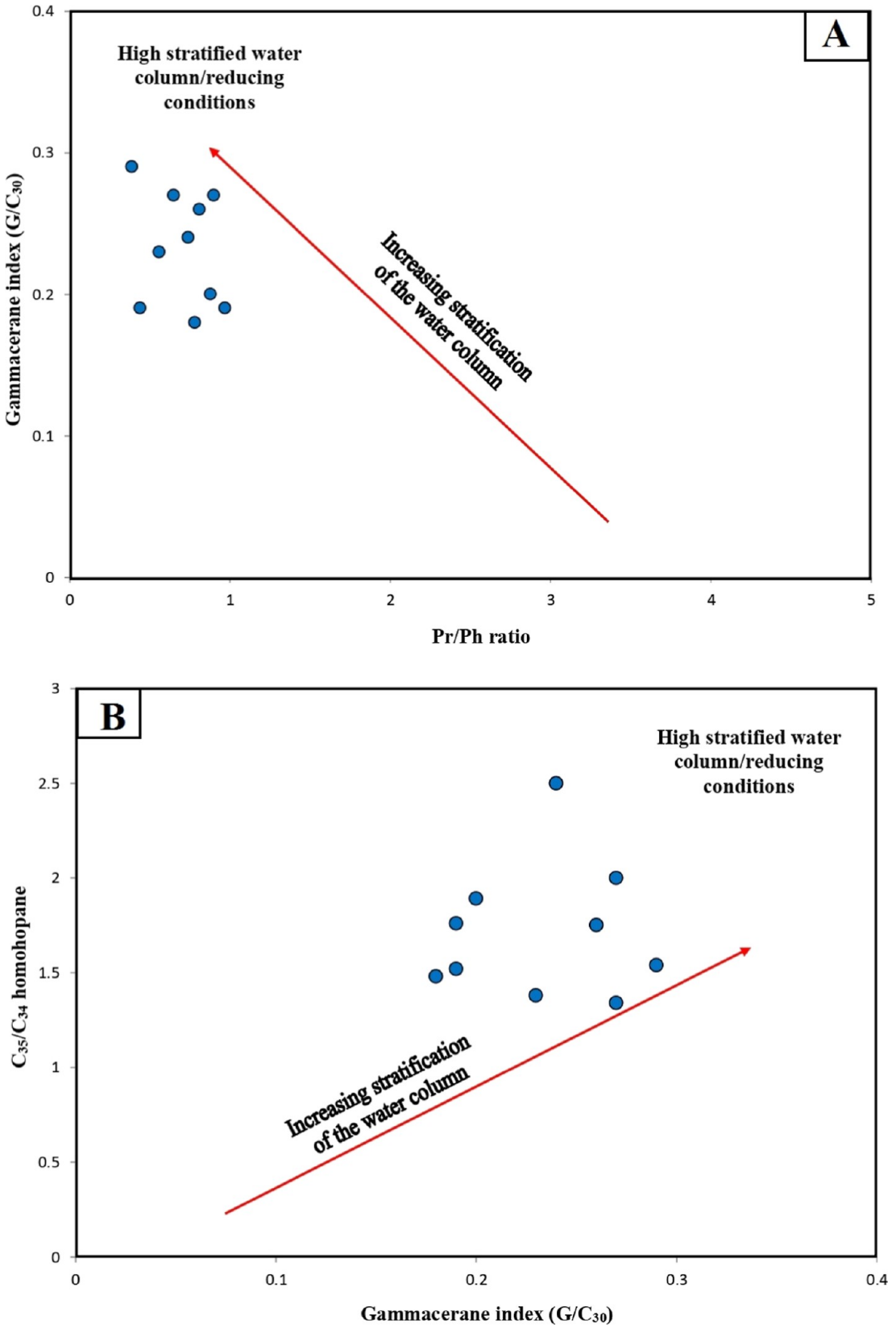

Figure 16. Geochemical biomarker results of the extracted bitumen from the studied bituminous carbonate rock in the Ajloun area, showing (A) Pr/Ph versus G/C_{30} and (B) G/C_{30} versus C_{35}/C_{34} homohopene, indicating stratification and anoxic conditions of the water columns.

relative changes in the proportions of silt to clay fractions.[83] In this case, the high Si/Al ratio indicates coarse grain size of clastic sediments during deposition.[66,84]

The studied Shu'ayb carbonate samples were characterized by a slightly lower average value of Si/Al ratio (1.33) than the UCC (4.33) and the post-Archaean Australian shale (PAAS, 3.32[85]).

https://doi.org/10.1021/acsomega.4c02582
ACS Omega 2024, 9, 27458−27479

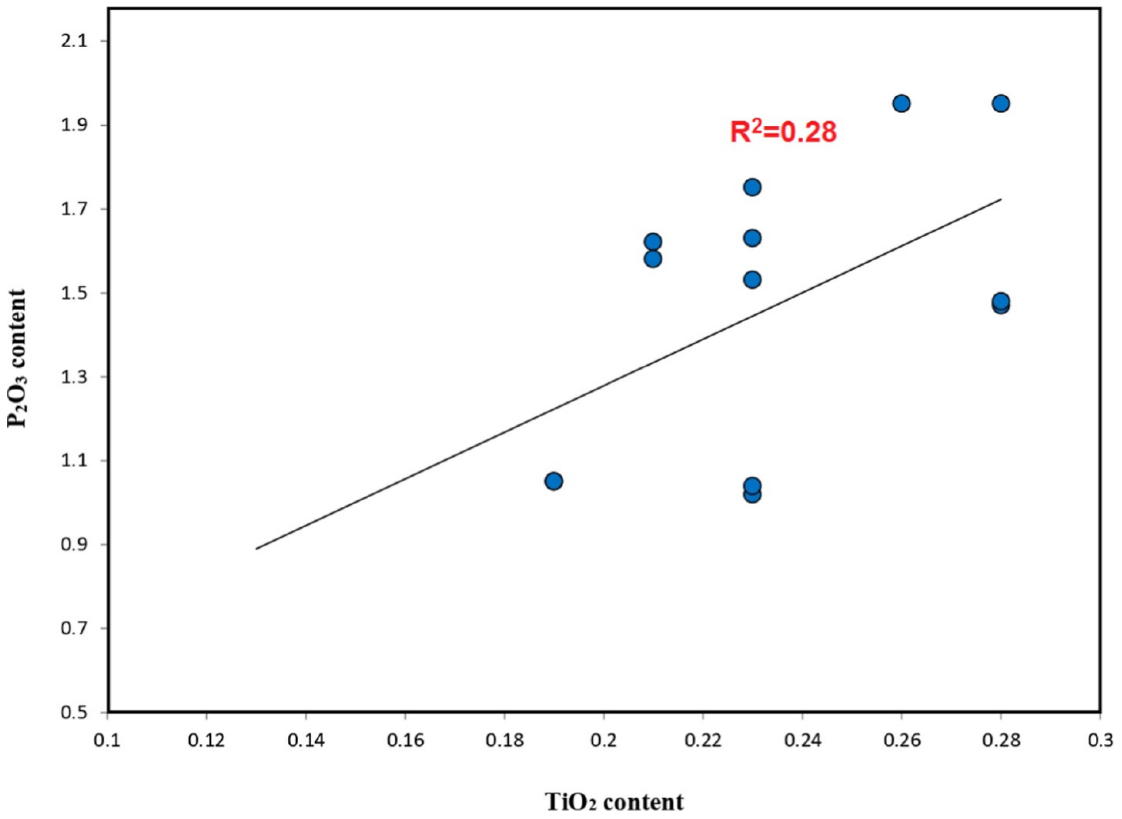

Figure 17. Cross-plot of the P_2O_3 and TiO_2 contents in the studied bituminous carbonate rock in the Ajloun area, showing weak correlation, and indicates that the P was sourced from OM.

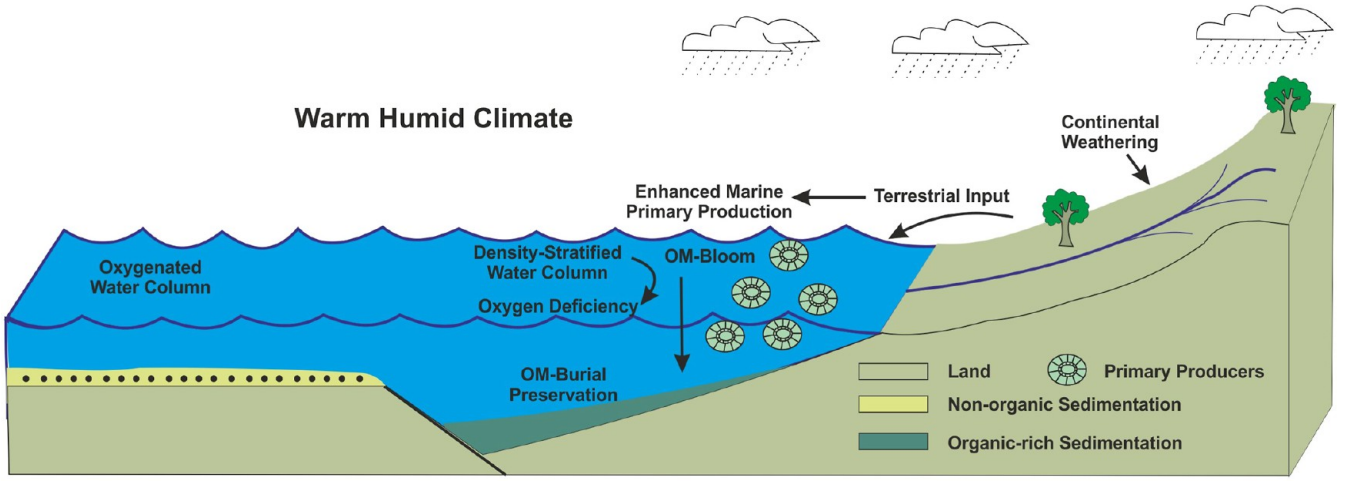

Figure 18. Paleoenvironmental model during deposition of the bituminous carbonate succession Upper Cretaceous Shu'ayb Formation.

This can be interpreted in terms of limited terrigenous supply during enhanced carbonate deposition of the Shu'ayb Formation. This is consistent with strong positive correlations between SiO_2 and Al_2O_3, as achieved from their R^2 of 0.77 (Figure 5A).

Further, the terrestrial influx can be estimated by aluminum (Al) and titanium (Ti) elements. Titanium (Ti) can be found in heavy minerals such as rutile (TiO_2) and ilmenite (FeTiO), while aluminum (Al) is common in feldspars and clay.[86] In this case, the Ti/Al ratio is the most applicable proxy to reflect the influence of terrestrial influx.[87] In this study, the Ti/Al ratios are below-average shale values ($Ti/Al_{\text{average shale}} = 0.046$), ranging from 0.02 to 0.04 (Table 1), due to the restriction in terrestrial input in the study area. Therefore, the detrital mineral input minimizes the effect of OM dilution, and therefore there was a high accumulation of OM throughout the time the Shu'ayb carbonate sediments were being deposited, as shown by the higher TOC contents than the detrital influx proxies and their Si/Al and Ti/Al ratios (Figure 6).

Further, the high Al/Al + Fe ratios between 0.87 and 0.89 are consistent with the Ti/Al ratio and show a terrestrial source because the Al/Al + Fe ratio of more than 0.4 indicates a terrestrial source,[88] reflecting a strong supply of nutrients from terrestrial sources into the ocean.

In addition, Fe/Ca + Mg ratios were investigated to know the approximate water depth, among which Ca and Mg are

https://doi.org/10.1021/acsomega.4c02582
ACS Omega 2024, 9, 27458−27479

commonly precipitated in carbonate and mud in deep water, while Fe, in an opposite way, can be found in terrigenous clastics.[89] Hence, the lower Fe/Ca + Mg ratios indicate a deeper setting. Accordingly, the Fe/Ca + Mg ratio in the Shu'ayb carbonate sediments has values of 0.02−0.03 (Table 2), referring to deep-water setting during their deposition.

5.6. Depositional Model of Organic Carbon Accumulation. Accumulation of organic-rich sediment within shallow basins during late Cretaceous is affected by the complex topographic relief of the basins.[90,91] In this context, the organic carbon accumulation in the studied bituminous carbonate succession of the Upper Cretaceous Shu'ayb Formation is controlled by different paleoenvironmental conditions and ecologic processes during deposition, as shown in Figure 18. This depositional model is characterized by low terrigenous input in a shallow-to-deep open marine environment (Figure 18). The terrigenous material originated from eroded bedrocks around the basin and was transported by freshwater input or wind flow.[92] In this case, fresh water flows toward the basin in the humid seasons pouncing stratification of water column in an estuarine system, where saline water trapped below the fresh water due to the existence of highland areas (swells).[93,94] In such situation, nutrients could be supplied from the continent through hydrologic cycles in humid and warm periods, and thereby the high marine primary productivity and enhanced riverine runoff in the basin likely induced enhanced water column stratification conditions (Figure 18). Those trapped water bodies were characterized by low oxygen content (Figure 18). This reduced bottom water condition, mainly anoxic, triggered high concentrations of total sulfur and TOC contents in the bituminous carbonate sediments of the Shu'ayb Formation (Figure 13). Therefore, predominantly redox conditions and water column stratification during the deposition of sediments that formed the Late Cretaceous Shu'ayb sequence in North Jordan triggered the enhanced preservation of organic carbon (Figure 18) and thereby contribute to OM enrichment.

Additionally, limited terrigenous supply during enhanced carbonate deposition of the Shu'ayb Formation provided favorable mineralogical conditions with an enhanced mineral surface area.[95] This conclusion is derived based on the low concentrations of terrestrial elements (i.e., SiO_2 and TiO_2) and their Si/Al and Ti/Al ratios, as shown in Table 1. Thus, the organic carbon-controlled processes during deposition of the Shu'ayb Formation enhanced the production and preservation versus limiting the dilution and decomposition of the available labile OM.[96]

6. CONCLUSIONS

Fifteen bituminous carbonate-rich samples of the upper Cretaceous Shu'ayb Formation taken from the Ajloun exposure in the Wadi Ajloun, Northern Jordan, were systematically analyzed. The OM input and the main sedimentary environmental conditions were assessed based on mainly geochemical results combined with microscopic examinations. The following conclusions can be summarized as follows:

- The Shu'ayb carbonate facies was deposited under anoxic marine environmental conditions with salinity stratification of the water column, as demonstrated by biomarker ratios, such as Pr/Ph, Pr/C_{17}, Ph/C_{18}, and gammacerane/C_{30} hopane (G/C_{30}) index, and high TOC and S contents together with the high abundance of marine organisms (i.e., lamalginite algae and foraminifera assemblages).
- Biomarker examinations together with carbon isotope analysis also revealed that the OM in the Shu'ayb bituminous carbonate rocks was derived from marine organisms, primarily phytoplankton algae, along with low amounts of terrestrial OM.
- The major elemental compositions show that the detrital influx was low in an open water depth system, ranging from deep shelf and slope to deep sea, with higher primary marine bioproductivity during deposition of the Shu'ayb bituminous carbonate rocks.
- The chemical index of alteration (CIA) values together with the high abundance of warm-water plankton species (i.e., *Globigerinoides* sp.) in the Shu'ayb bituminous carbonate facies showed intense subaerial weathering due to the hot and humid paleoclimatic conditions, resulting in an increase in the nutrient level in the sea surface, which caused the high bioproductivity of the phytoplankton.

APPENDIX

Peak assignments for hydrocarbons in the gas chromatograms of saturated fractions in the *m/z* 191 (I) and 217 (II) mass fragmentograms (used for reference to explain Figure 8) are given in Table A1.

Table A1

peak no.	compound	abbreviation
(I) *m/z* 191		
Ts	18α(H),22,29,30-trisnorneohopane	Ts
Tm	17α(H),22,29,30-trisnorhopane	Tm
29	17α,21β(H)-nor-hopane	C_{29} hop
30	17α,21β(H)-hopane	Hopane
30M	17 β,21α (H)-moretane	C_{30}Mor
31S	17α,21β(H)-homohopane (22S)	C_{31}(22S)
31R	17α,21β(H)-homohopane (22R)	C_{31}(22R)
32S	17α,21β(H)-homohopane (22S)	C_{32}(22S)
32R	17α,21β(H)-homohopane (22R)	C_{32}(22R)
33S	17α,21β(H)-homohopane (22S)	C_{33}(22S)
33R	17α,21β(H)-homohopane (22R)	C_{33}(22R)
34S	17α,21β(H)-homohopane (22S)	C_{34}(22S)
34R	17α,21β(H)-homohopane (22R)	C_{34}(22R)
(II) *m/z* 217		
a	13β,17α(H)-diasteranes 20S	diasteranes
b	13β,17α(H)-diasteranes 20R	diasteranes
c	13α,17β(H)-diasteranes 20S	diasteranes
d	13α,17β(H)-diasteranes 20R	diasteranes
e	5α,14α(H), 17α(H)-steranes 20S	$\alpha\alpha\alpha$20S
f	5α,14β(H), 17β(H)-steranes 20R	$\alpha\beta\beta$20R
g	5α,14β(H), 17β(H)-steranes 20S	$\alpha\beta\beta$20S
h	5α,14α(H), 17α(H)-steranes 20R	$\alpha\alpha\alpha$20R

AUTHOR INFORMATION

Corresponding Author

Mohammed Hail Hakimi − *Geology Department, Faculty of Applied Science, Taiz University, 6803 Taiz, Yemen;* orcid.org/0000-0002-3320-9690; Email: ibnalhakimi@yahoo.com

https://doi.org/10.1021/acsomega.4c02582
ACS Omega 2024, 9, 27458−27479

Authors

Mohammad Alqudah − *Department of Earth and Environmental Sciences, Yarmouk University, 21163 Irbid, Jordan;* orcid.org/0000-0002-5255-8394

Malik M. Momani − *Ministry of Education, Amman 11118, Jordan*

Danish Zahir − *Department of Geology, University of Poonch Rawalakot, Azad Jammu& Kashmir Rawalakot 12350, Pakistan*

Ahmed Abd El Aal − *Faculty of Engineering, Civil Engineering Department, Najran University, Najran 61441, Saudi Arabia*

Mohamed M. El Nady − *Exploration Department, Egyptian Petroleum Research Institute (EPRI), Nasr City 11727 Cairo, Egypt;* orcid.org/0000-0003-4269-0620

Afikah Rahim − *Department of Geotecnics & Transportation, Faculty of Civil Engineering, Universiti Teknologi Malaysia, 81310 Johor Bahru, Malaysia*

Baleid Ali Hatem − *Department of Geology, University of Malaya, 50603 Kuala Lumpur, Malaysia*

Complete contact information is available at: https://pubs.acs.org/10.1021/acsomega.4c02582

Notes

The authors declare no competing financial interest.

■ ACKNOWLEDGMENTS

The authors would also like to express their gratitude to the administration of the University of Malaya's Department of Geology for providing the facilities for organic geochemistry and petrographic investigations.

■ REFERENCES

(1) Hackley, P. C.; Ryder, R. T. Organic geochemistry and petrology of Devonian shale in eastern Ohio: Implications for petroleum systems assessment. *Am. Assoc. Petrol. Geol. Bull.* **2021**, *105* (3), 543−573.

(2) Sohail, G. M.; Radwan, A. E.; Mahmoud, M. A review of Pakistani shales for shale gas exploration and comparison to North American shale plays. *Energy Rep.* **2022**, *8*, 6423−6442.

(3) Qadri, S. M. T.; Shalaby, M. R.; Islam, M. A.; Hoon, L. L. Source rock characterization and hydrocarbon generation modeling of the Middle to Late Eocene Mangahewa Formation in Taranaki Basin, New Zealand. *Arabian J. Geosci.* **2016**, *9*, 559.

(4) Jarvie, D. M.; Hill, R. J.; Ruble, T. E.; Pollastro, R. M. Unconventional shale-gas systems: The Mississippian Barnett Shale of north-central Texas as one model for thermogenic shale-gas assessment. *Am. Assoc. Petrol. Geol. Bull.* **2007**, *91* (4), 475−499.

(5) Abd El Gawad, E. A.; Makled, W. A.; Mousa, A. S.; El Hariri, T. Y.; Mousa, D. A.; Hamed, T. E. Relationship between cyclic patterns of organic matter concentrations and their paleoenvironmental controls in the Upper Cretaceous rocks in Abu El Gharadig basin, Egypt: Cyclo-sequence stratigraphic framework. *Mar. Petrol. Geol.* **2022**, *136*, 105474.

(6) Liu, X.; Chen, H.; Mu, X.; Zhang, H.; Fan, J.; Huang, Y.; Zhao, K.; Mansour, A.; Gentzis, T.; Ostadhassan, M. Organic matter preservation conditions in the third member of the Shahejie Formation (Dongpu Depression, China). *Int. J. Coal Geol.* **2023**, *277*, 104334.

(7) Mansour, A.; Wagreich, M. *An overview of the Cretaceous oceanic anoxic events in Egypt, southern Tethys*; Special Publications, Geological Society: London, 2024; .

(8) Li, T. Y.; He, S.; Yang, Z. The marine source rock formation conditions and control factors. *Geol. Sci. Technol. Inf.* **2008**, *27*, 63−70. In Chinese with English abstract

(9) Zonneveld, K. A. F.; Versteegh, G. J. M.; Kasten, S.; Eglinton, T. I.; Emeis, K. C.; Huguet, C.; Koch, B. P.; de Lange, G. J.; de Leeuw, J. W.; Middelburg, J. J.; et al. Selective preservation of organic matter in marine environments; processes and impact on the sedimentary record. *Biogeosciences* **2010**, *7*, 483−511.

(10) Bechtel, A.; Jia, J. L.; Strobl, S. A. I.; Sachsenhofer, R. F.; Liu, Z. J.; Gratzer, R.; Püttmann, W. Palaeoenvironmental conditions during deposition of the Upper Cretaceous oil shale sequences in the Songliao Basin (NE China): Implications from geochemical analysis. *Org. Geochem.* **2012**, *46*, 76−95.

(11) Tao, S.; Tang, D.; Xu, H.; Liang, J.; Shi, X. Organic geochemistry and elements distribution in Dahuangshan oil shale, southern Junggar Basin: Origin of organic matter and depositional environment. *Int. J. Coal Geol.* **2013**, *115*, 41−51.

(12) Alali, J. (2006). Jordan Oil Shale, Availability, Distribution, and Investment Opportunity. *International Conference on Oils Shale: "Recent Trends in Oil Shale"*, Amman, 7−9 November 2006, Paper No. rtos-A117.

(13) Aqleh, S.; van den Boorn, S.; Podlaha, O. G.; Marz, C.; Wagner, T.; Poulton, S.; Kolonic, S. Reconstruction of redox conditions during deposition of Jordan oil shale using inorganic geochemical records. *Mineral. Mag.* **2013**, *77*, 603.

(14) Hussein, M. A.; Alqudah, M.; Podlaha, O. Ichnofabrics of Eocene oil shales from central Jordan and their use for paleoenvironmental reconstructions. *GeoArabia* **2014**, *19*, 85−112.

(15) Alqudah, M.; Ali Hussein, M.; van den Boorn, S.; Giraldo, V. M.; Kolonic, S.; Podlaha, O. G.; Mutterlose, J. Eocene oil shales from jordan—Paleoenvironmental implications from reworked microfossils. *Mar. Petrol. Geol.* **2014**, *52*, 93−106.

(16) Ali Hussein, M.; Alqudah, M.; Blessenohl, M.; Podlaha, O. G.; Mutterlose, J. Depositional environment of Late Cretaceous to Eocene organic-rich marls from Jordan. *GeoArabia* **2015**, *20*, 191−210.

(17) Hakimi, M. H.; Abdullah, W. H.; Alqudah, M.; Makeen, Y. M.; Mustapha, K. A. Reducing marine and warm climate conditions during the Late Cretaceous, and their influence on organic matter enrichment in the oil shale deposits of North Jordan. *Int. J. Coal Geol.* **2016**, *165*, 173−189.

(18) Hakimi, M. H.; Abdullah, W. H.; Alqudah, M.; Makeen, Y. M.; Mustapha, K. A.; Hatem, B. A. Pyrolysis analyses and bulk kinetic models of the Late Cretaceous oil shales in Jordan and their implications for early mature sulphur-rich oil generation potential. *Mar. Petrol. Geol.* **2018**, *91*, 764−775.

(19) Hakimi, M. H.; Alqudah, M.; Mustapha, K. A.; Varfolomeev, M. A.; Lashin, A.; Hatem, B. A.; Rahim, A.; Sen, S.; Radwan, A. E.; Yelwa, N. A. Early-oil generation potential of Type II-S kerogen in the Upper Cretaceous (Cenomanian−Turonian) organic-rich carbonate succession from Ajloun region in northern Jordan. *Arabian J. Sci. Eng.* **2023**, *48*, 695−710.

(20) Powell, J. H.; Moh'd, B. Evolution of Cretaceous to Eocene alluvial and carbonate platform sequences in central and south Jordan. *GeoArabia* **2011**, *16* (4), 29−82.

(21) Abed, A. Emergence of Wadi Mujib (Central Jordan) during Lower Cenomanian time and its regional tectonic implications; Special Publications, Geological Society: London, 1984; Vol. *17*, pp 213−216..

(22) Alsharhan, A. S.; Nairn, A. E. M. *Sedimentary basins and petroleum geology of the Middle East*; Elsevier: Amsterdam, 1997; p 843.

(23) Schulze, F.; Marzouk, A. M.; Bassiouni, M. A.; Kuss, J. The late Albian−Turonian carbonate platform succession of west-central Jordan: stratigraphy and crises. *Cretaceous Res.* **2004**, *25* (5), 709−737.

(24) Abdelhamid, G., 1993. Geological map of Jarash (Unpublished map). Ministry of Energy and Mineral Resources - Natural Resources Authority (NRA) (Geology directorate). *National mapping project*. Map sheet No. (3154-I); 1 sheet: 1:50.000. Amman, Jordan.

(25) Masri, A., 2003. The geology of the Dhiba (Wadi Al-Mujib area map sheet, *National Mapping Project*, Bulletin 54 No. 3152-i. Natural Resources Authority, Amman.

(26) Al-Rifaiy, I. A.; Cherif, O. H. Biostratigraphic aspects and regional correlation of some Cenomanian−Turonian exposures in Jordan, 1987, pp 181−193..*In: geolm.14*

(27) Sawariah, A.; Barjous, M. *Geological Map Suwaylih Scale 1:50,000, sheet no.3154-II (unpublished map)*; Natural Resources Authority: Amman, Jordan, 1993.

https://doi.org/10.1021/acsomega.4c02582
ACS Omega 2024, 9, 27458−27479

(28) Abdelhamid, G. The geology of Jarash Area (Unpublished report). Hashemite Kingdom of Jordan; Ministry of Energy and Mineral Resources; Natural Resources Authority, Geology Directorate, Geological Mapping Division, 1995.
(29) Taylor, G.; Teichmüller, M.; Davis, A.; Diessel, C.; Littke, R.; Robert, P. Organic Petrology; Gebrüder Bornatraeger: Berlin-Stuttgart, 1998; p 704.
(30) Tissot, B. P.; Welte, D. H. *Petroleum Formation and Occurrence*; Springer-Verlag: New York, 1984; p 699.
(31) Hakimi, M. H.; Abdullah, W. H.; Shalaby, M. R. Geochemical and petrographic characterization of organic matter in the Upper Jurassic Madbi shale succession (Masila Basin, Yemen): origin, type and preservation. *Org. Geochem.* **2012**, *49*, 18−29.
(32) Berner, R. A.; Raiswell, R. Burial of organic carbon and pyrite sulfur in sediments over Phanerozoic time: a new theory. *Geochim. Cosmochim. Acta* **1983**, *47*, 855−862.
(33) Wei, W.; Algeo, T. J. Elemental proxies for paleosalinity analysis of ancient shales and mudrocks. *Geochem. Cosmochim. Acta.* **2020**, *287*, 341−366.
(34) Sofer, Z. Stable carbon isotope compositions of crude oils: application to source depositional environments and petroleum alteration. *Am. Assoc. Petrol. Geol. Bull.* **1984**, *68*, 31−49.
(35) Summons, R. E.; Thomas, J.; Maxwell, J. R.; Boreham, C. J. Secular and environmental constraints on the occurrence of dinosterane in sediments. *Geochim. Cosmochim. Acta* **1992**, *56*, 2437−2444.
(36) Mukhopadhyay, P. K.; Goodarzi, F.; Crandlemire, A. L.; Gillis, K. S.; MacNeil, D. J.; Smith, W. D. Comparison of coal composition and elemental distribution in selected seams of the Sydney and Stellarton Basins, Nova Scotia, Eastern Canada. *Int. J. Coal Geol.* **1998**, *37*, 113−141.
(37) Fu, X.; Wang, J.; Zeng, Y.; Tan, F.; Feng, X. REE geochemistry of marine oil shale from the Changshe Mountain area, northern Tibet, China. *Int. J. Coal Geol.* **2010**, *81*, 191−199.
(38) Fu, X.; Wang, J.; Zeng, Y.; Cheng, J.; Tan, F. Origin and mode of occurrence of trace elements in marine oil shale from the Shengli River Area. *Northern Tibet, China. Oil Shale* **2011**, *28*, 487.
(39) Ross, D. J. K.; Bustin, R. M. Investigating the use of sedimentary geochemical proxies for paleoenvironment interpretation of thermally mature organic-rich strata: Examples from the Devonian−Mississippian shales, Western Canadian Sedimentary Basin. *Chem. Geol.* **2009**, *260*, 1−19.
(40) Didyk, B. M.; Simoneit, B. R. T.; Brassell, S. C.; Eglinton, G. Organic geochemical indicators of palaeoenvironmental conditions of sedimentation. *Nature* **1978**, *272*, 216−222.
(41) Chandra, K.; Mishra, C. S.; Samanta, U.; Gupta, A.; Mehrotra, K. L. Correlation of different maturity parameters in the Ahmedabad−Mehsana block of the Cambay basin. *Org. Geochem.* **1994**, *21*, 313−321.
(42) Pu, F.; Philip, R.; Zhenxi, L.; Guangguo, Y. Geochemical characteristics of aromatic hydrocarbons of crude oils and source rocks from different sedimentary environments. *Org. Geochem.* **1990**, *16*, 427−435.
(43) Hughes, W.; Holba, A. G.; Dzou, L. The ratios of dibenzothiophene to phenanthrene and pristane to phytane as indicators of depositional environment and lithology of petroleum source rocks. *Geochim. Cosmochim. Acta* **1995**, *59*, 3581−3598.
(44) Waples, D. W.; Machihara, T. *Biomarkers for Geologists: A Practical Guide to the Application of Steranes and Triterpanes in Petroleum Geology*; American Association of Petroleum Geologists Methods in Exploration 9: Tulsa, OK, 1991; .
(45) Murray, A. P.; Boreham, C. J. Organic geochemistry in petroleum exploration. *Aust. Geol. Surv. Organ. Canberra* **1992**, *230*.
(46) Zumberge, J. E. Terpenoid biomarker distributions in low maturity crude oils. *Org. Geochem.* **1987**, *11*, 479−496.
(47) Hadad, Y. T.; Hakimi, M. H.; Abdullah, W. H.; Kinawy, M.; El Mahdy, O.; Lashin, A. Organic geochemical characteristics of Zeit source rock from Red Sea Basin and their contribution to organic matter enrichment and hydrocarbon generation potential. *J. African Earth Sci.* **2021**, *177*, 104151.
(48) Huang, W. Y.; Meinschein, W. G. Sterols as ecological indicators. *Geochem. Cosmochim. Acta.* **1979**, *43*, 739−745.
(49) Dean, W. E.; Arthur, M. A. Iron-sulfur-carbon relationships in organic-carbon-rich sequences I: cretaceous western interior seaway. *Am. J. Sci.* **1989**, *43* (6), 289−708.
(50) Escobar, M.; Márquez, G.; Inciarte, S.; Rojas, J.; Esteves, I.; Malandrino, G. The organic geochemistry of oil seeps from the Sierra de Perijá eastern foothills, Lake Maracaibo Basin, Venezuela. *Venezuela. Org. Geochem.* **2011**, *42*, 727−738.
(51) Ten Haven, H. L.; De Leeuw, J. W.; Rullkötter, J.; Damsté, J. S. S. Restricted utility of the pristane/phytane ratio as a palaeoenvironmental indicator. *Nature* **1987**, *330*, 641−643.
(52) Large, D. J.; Gize, A. P. Pristane/phytane ratios in the mineralized Kupferschiefer of the Fore-Sudetic Monocline, southwest Poland. *Ore Geol. Rev.* **1996**, *11*, 89−103.
(53) Xu, J.; Liu, Z.; Bechtel, A.; Meng, Q.; Sun, P.; Jia, J.; Cheng, L.; Song, Y. Basin evolution and oil shale deposition during Upper cretaceous in the songliao basin (NE China): Implications from sequence stratigraphy and geochemistry. *Int. J. Coal Geol.* **2015**, *149*, 9−23.
(54) Lei, B.-J.; Que, H. P.; Hu, N.; Niu, Z. J.; Wang, H. Geochemistry and sedimentary environments of the Palaeozoic siliceous rocks in western Hubei. *Sediment. Geol. Tethyan Geol.* **2002**, *22* (2), 70−79. In Chinese with English Abstract
(55) Zhang, K.; Liu, R.; Liu, Z.; Li, B.; Han, J.; Zhao, K. Influence of volcanic and hydrothermal activity on organic matter enrichment in the Upper Triassic Yanchang Formation, southern Ordos Basin, Central China. *Mar. Petrol. Geol.* **2020**, *112*, 104059.
(56) Xu, X.-T.; Shao, L.-Y.; Eriksson, K. A.; Pang, B.; Wang, S.; Yang, C.-X.; Hou, H.-H. Terrestrial records of the early Albian Ocean Anoxic Event: Evidence from the Fuxin lacustrine basin, NE China. *NE China. Geosci. Front.* **2022**, *13*, 101275.
(57) Lan, X. H.; Ma, D. X.; Xu, M. G.; et al. Some geochemical signs and their importance for sedimentary facies. *Mar. Geol. Quat. Geol.* **1987**, *7* (1), 39. in Chinese with English Abstract
(58) Hu, X. F.; Liu, Z. J.; Liu, R.; et al. Clay mineral and inorganic geochemical characteristics of Eocene Huadian formation in Huadian Basin and their paleoenvironment implications. *J. China Coal Soc.* **2012a**, *37* (3), 416−423. in Chinese with English Abstract
(59) Sinninghe Damsté, J. S.; Kenig, F.; Koopmans, M. P.; Koster, J.; Schouten, S.; Hayes, J. M.; de Leeuw, J. W. Evidence for gammacerane as an indicator of water column stratification. *Geochim. Cosmochim. Acta* **1995**, *59*, 1895−1900.
(60) Felix, N. S. Physico-chemical studies on bentonites with special reference to Fayoum Deposits. Ph.D. Thesis, Faculty of Science, Cairo University, Egypt, 1977.
(61) Moradi, A. V.; Sari, A.; Akkaya, P. Geochemistry of the miocene oil shale (Hanili Formation) in the ankr-orum basin, Central Turkey: implications for paleoclimate conditions, source−area weathering, provenance and tectonic setting. *Sediment. Geol.* **2016**, *341* (2), 289−303.
(62) Niebuhr, B. Geochemistry and time-series analyses of orbitally forced Upper Cretaceous marl-limestone rhythmites (Lehrte West Syncline, northern Germany). *Geol. Mag.* **2005**, *142*, 31−55.
(63) Mansour, A.; Wagreich, M.; Gier, S.; Gentzis, T.; Kloetzli, U.; Tahoun, S. S.; Elewa, A. M. T. Climate variability and paleoceanography during the Late Cretaceous: Evidence from palynology, geochemistry and stable isotopes analyses from the southern Tethys. *Cretaceous Res.* **2021**, *126* (126), 104831.
(64) Hieronymus, B.; Kotschoubey, B.; Boulegue, J. Gallium behaviour in some contrasting lateritic profiles from Cameroon and Brazil. *J. Geochem. Explor.* **2001**, *72*, 147−163.
(65) Beckmann, B.; Flögel, S.; Hofmann, P.; Schulz, M.; Wagner, T. Orbital forcing of Cretaceous river discharge in tropical Africa and ocean response. *Nature* **2005**, *437*, 241−244.
(66) Ratcliffe, K. T.; Wright, A. M.; Hallsworth, C.; Morton, A.; Zaitlin, B. A.; Potocki, D.; Wray, D. S. Alternative correlation techniques in the petroleum industry: an example from the (Lower

https://doi.org/10.1021/acsomega.4c02582
ACS Omega 2024, 9, 27458−27479

Cretaceous) Basal Quartz, Southern Alberta. *Bull. Am. Assoc. Pet. Geol.* **2004**, *88*, 419−432.
(67) Xia, G.; Mansour, A. Paleoenvironmental changes during the early Toarcian Oceanic Anoxic Event: Insights into organic carbon distribution and controlling mechanisms in the eastern Tethys. *J. Asian Earth Sci.* **2022**, *237*, 105344.
(68) Nesbitt, H. W.; Young, G. M. Early proterozoic climates and plate motions inferred from major element chemistry of lutites. *Nature* **1982**, *299*, 715−717.
(69) Bahlburg, H. A review of the Chemical Index of Alteration (CIA) and its application to the study of Neoproterozoic glacial deposits and climate transitions. In *The Geological Record of Neoproterozoic Glaciations*; Arnaud, E., Halverson, G. P., Shields, G. A., Eds.; Geological Society of London: Memoir, 2009; Vol. *36*, pp 81−91.
(70) Wang, P.; Du, Y.; Yu, W.; Algeo, T. J.; Zhou, Q.; Xu, Y.; Qi, L.; Yuan, L.; Pan, W. The chemical index of alteration (CIA) as a proxy for climate change during glacial- interglacial transitions in earth history. *Earth Sci. Rev.* **2020**, *201*, 103032.
(71) Michal, K. Planktonic foraminifera as tracers of past oceanic environments. *Dev. Mar. Geol.* **2007**, *1*, 213−262.
(72) Murray, J. On the distribution of the pelagic foraminifera at the surface and on the floor of the ocean. *Nat. Sci.* **1897**, *11* (65), 17−27.
(73) Rutherford, S.; D'Hondt, S.; Prell, W. Environmental controls on the geographic distribution of zooplankton diversity. *Nature* **1999**, *400*, 749−753.
(74) Schmidt, D. N.; Renaud, S.; Bollmann, J.; Schiebel, R.; Thierstein, H. R. Size distribution of Holocene planktic foraminifer assemblages: biogeography, ecology and adaptation. *Mar. Micropaleontol.* **2004**, *50*, 319−338.
(75) Gallagher, S. J.; Greenwood, D. R.; Taylor, D.; Smith, A. J.; Wallace, M. W.; Holdgate, G. R. The Pliocene climatic and environmental evolution of southeastern Australia: evidence from the marine and terrestrial realm. *Palaeogeogr. Palaeoclimatol. Palaeoecol.* **2003**, *193*, 349−382.
(76) Liu, P.; Liu, C.; Guo, R. Depositional Environment and Organic Matter Enrichment in the Lower Paleozoic Shale from the Northeastern Margin of the Yangtze Platform, South China. *J. Mar. Sci. Eng.* **2023**, *11* (3), 501.
(77) Yang, M.; Zuo, Y.; Fu, X.; Qiu, L.; Li, W.; Zhang, J.; Zheng, Z.; Zhang, J. Paleoenvironment of the Lower Ordovician Meitan Formation in the Sichuan Basin and Adjacent Areas, China. *China. Minerals* **2022**, *12*, 75.
(78) Mansour, A.; Gentzis, T.; Ied, I. M.; Ahmed, M. S.; Wagreich, M. Paleoenvironmental Conditions and Factors Controlling Organic Carbon Accumulation during the Jurassic−Early Cretaceous, Egypt: Organic and Inorganic Geochemical Approach. *Minerals* **2022**, *12*, 1213.
(79) Soua, M.; Zaghbib-Turki, D.; Ben Jemia, H.; Smaoui, J.; Boukadi, A. Geochemical record of the Cenomanian-Turonian anoxic event in Tunisia: Is it correlative and isochronous to the biotic signal? *Acta Geol. Sin.* **2011**, *85* (6), 1310−1335.
(80) Bai, Y.; Liu, Z.; Sun, P.; Liu, R.; Hu, X.; Zhao, H.; Xu, Y. Rare earth and major element geochemistry of Eocene fine-grained sediments in oil shale-and coal-bearing layers of the Meihe Basin, Northeast China. *J. Asian Earth Sci.* **2015**, *97*, 89−101.
(81) Algeo, T. J.; Maynard, J. B. Trace-element behavior and redox facies in core shales of Upper Pennsylvanian Kansas-type cyclothems. *Chem. Geol.* **2004**, *206*, 289−318.
(82) Maravelis, A. G.; Offler, R.; Pantopoulos, G.; Collins, W. J. Provenance and tectonic setting of the early permian sedimentary succession in the southern edge of the Sydney Basin, eastern Australia. *Geol. J.* **2021**, *56*, 2258−2276.
(83) Ratcliffe, K.; Wright, A. M.; Spain, D. R. Unconventional methods for unconventional plays: Using elemental data to understand shale resource plays. *Pet. Explor. Soc. Aust. News Res.* **2012**, *117*, 50−54.
(84) LaGrange, M. T.; Konhauser, K. O.; Catuneanu, O.; Harris, B. S.; Playter, T. L.; Gingras, M. K. Sequence stratigraphy in organic-rich marine mudstone successions using chemostratigraphic datasets. *Earth-Sci. Rev.* **2020**, *203*, 103137.
(85) Taylor, S. R.; McLennan, S. M. *The Continental Crust: Its Composition and Evolution*; Oxford : Blackwell Scientific: Malden, MA, USA, 1985; .
(86) Rimmer, S. M.; Thompson, J. A.; Goodnight, S. A.; Robl, T. L. Multiple controls on the preservation of organic matter in devonian mississippian marine black shales: geochemical and petrographic evidence. *Palaeogeogr. Palaeoclimatol. Palaeoecol.* **2004**, *215*, 125−154.
(87) Murphy, A. E.; Sageman, B. B.; Hollander, D. J.; Lyons, T. W.; Brett, C. E. Black shale deposition and faunal overturn in the devonian appalachian basin: clastic starvation, seasonal water-column mixing, and efficient biolimiting nutrient recycling. *Paleoceanography* **2000**, *15* (3), 280−291.
(88) Liu, Z. H.; Zhuang, X. G.; Teng, G. E.; Xie, X. M.; Yin, L. M.; Bian, L. Z.; Feng, Q.; Algeo, T. The lower cambrian niutitang formation at yangtiao (Guizhou, SW China): organic matter enrichment, source rock potential, and hydrothermal influences. *J. Pet. Geol.* **2015**, *38*, 411−432.
(89) Chen, Z.; Huang, W.; Liu, Q.; Zhang, L.; Zhang, S. Geochemical characteristics of the paleogene shales in the Dongying depression, eastern China. *Mar. Petrol. Geol.* **2016**, *73*, 249−270.
(90) Alqudah, M.; Ali Hussein, M.; van den Boorn, S.; Podlaha, O. G.; Mutterlose, J. Biostratigraphy and depositional setting of Maastrichtian—Eocene oil shales from Jordan. *Mar. Pet. Geol.* **2015**, *60*, 87−104.
(91) Hussein, A.; Al-Tarawneh, O. M.; Alqudah, M. Calcareous Nannofossils Biostratigraphy of Late Cretaceous−Paleocene Successions from Northern Jordan and Their Implications for Basin Analysis. *Geosciences* **2023**, *13*, 351.
(92) Kong, X.; Jiang, Z.; Ju, B.; Liang, C.; Cai, Y.; Wu, S. Fine-grained carbonate formation and organic matter enrichment in an Eocene saline rift lake (Qianjiang Depression): constraints from depositional environment and material source. *Mar. Pet. Geol.* **2022**, *138*, 105534.
(93) Abed, A. The eastern Mediterranean phosphorite giants: An interplay between tectonics and upwelling. *GeoArabia* **2013**, *18*, 67−94.
(94) Alqudah, M.; Al Alaween, M.; Fermor, A.; Ali, E.; Wagner, T.; Alhakimi, M. H.; Rahim, A. Impact of Thermal Maturation of the Upper Cretaceous Bituminous Limestone of Attarat Um Ghudran Central Jordan on Calcareous Nannofossil Preservation. *ACS Omega* **2023**, *8* (42), 39830−39846.
(95) Kennedy, M. J.; Wagner, T. Clay mineral continental amplifier for marine carbon sequestration in a greenhouse ocean. *Proc. Natl. Acad. Sci. U.S.A.* **2011**, *108*, 9776−9781.
(96) Tyson, R. V. The "productivity versus preservation" controversy: cause, flaws and resolution. In *The deposition of organic-carbon-rich sediments: models, mechanisms, and consequences*; Harris, N. B., Ed.; SEPM Special Publication, 2011; Vol. *82*, pp 17−33..

https://doi.org/10.1021/acsomega.4c02582
ACS Omega 2024, 9, 27458−27479